NTNU

Norwegian University of
Science and Technology

Intercalation of CO_2, water and diglyme in MXenes using molecular simulations

Alexander Bjørlo

Chemical Engineering and Biotechnology
Submission date: July 2018
Supervisor: Sondre Kvalvåg Schnell, IMA
Co-supervisor: Jacob Hadler-Jacobsen, IMT

Norwegian University of Science and Technology
Department of Materials Science and Engineering

Summary

Since its discovery in 2011, MXenes have gained a lot of attention for their application in energy storage. Their combination of being a two dimensional material, as well as having excellent electronic and mechanical properties, makes them an interesting material for electronic energy storages, as well as for CO_2 capture. This is emphasized the weak Van der Waals forces between the layers. Both small ions and large organic molecules have been successfully intercalated between the MXene layers. MXenes are hydrophilic, and water intercalate easily between their layer. This can be problematic for its applications in energy storage, where water may be present.

This study investigates the adsorption properties of Ti_2C MXenes terminated with Fluor and Oxygen. This is done using Monte Carlo methods and Molecular dynamics simulations in the osmotic ensable. The adsorbates studied are the two water models SPC/E and TIP5p, Diglyme and CO_2. The simulations are performed at small pressure discretizations in a flexible multilayered MXene framework. The simulations are performed with the software package RASPA. The simulations show many uncertainties, allthough some results were gathered. The adsorption of water was found to be higher than the adsorption of CO_2, which corresponds well with the hydrophilic nature of MXenes. Results suggests that the adsorption was a physical adsorption, by evaluating the isosteric heat of adsorption, although the isosteric heat of adsorption shows nonphysical behaviour. Diglyme was not adsorbed to the framework at any temperatures, which most likely is due to the unit cell volume being close to constant throughout the simulation. This is the case for all of the adsorbate-adsorbent systems simulated. The adsroption of SPC/E water, TIP5p water and CO_2 were most likely limited by kintetics at low temperatures, and thermodynamics at high temperatures. This contradicts with the Monte Carlo methods, which should not be restricted by kinetics. The simulations performed, although some evidence of adsorption were observed, are most likely not of any significance. This is due to several nonphysical phenomena observed. These phenomena are probably due to too few Monte Carlo cycles, and viable results may be obtained using several more cycles.

Sammendrag

Siden oppdagelsen i 2011, har MXener fått mye oppmerksomhet som materiale til anvendelse i energilagring. Kombinasjonen av at det er et todimensjonalt materiale, samtidig som det har umterkede mekaniske og elektroniske egenskaper, gjør at det er et interesangt materiale å anvende til energilagring, så vel som for CO_2 fangst. Dette er underbygget av de svake Van der Waals kreftene som virker mellom lagene. Både små ioner og store organiske molekyler har blitt interkalert mellom MXene lagene. MXener er hydrofile, og vann interkalerer lett mellom lagene. Dette kan være problematisk for bruk i energilagring, hvor vann kan være til stede.

Denne studien undersøker adsorpsjonsegenskapene til Ti_2C MXene terminert med fluor og oksygen. Dette er gjort ved bruk av monte carlo metoder, og molecular dynamics simuleringer, i det osmotiske ensemble. Adsorbatene som blir undersøkt er de to vannmodellene SPC/E og TIP5p, Diglyme og CO_2. Simuleringene blir utført på små trykkdiskretiseringer i en fleksibel mangelags MXene. Simuleringene blir utført med softwarepakken RASPA. Simuleringene viste mange usikkerhetsmomenter, dog ble noen trender observet. Adsorbsjonen til vann ble funnet til å være større en adsorbsjonen til CO_2, som underbygger de hydrofile egenskapene til MXener. Resultatene foreslår at adsorpsjonen som ble observert var fysisk adsorbjon, ved å undersøke den isosteriske adsorbsjonsvarmen. Det må dog nevnes at den isosteriske adsorbsjonsvarmen viser tegn til ufysisk oppførsel. Diglyme ble ikke adsorbert i MXenlagene. Dette er mest sannsynlig grunnet volumet av enhetscellen, som viste seg å være tilnærmet konstant gjennom simuleringene. Dette gjelder for alle adsorbat-adsorbent systemene simulert. Adsorbsjonen av SPC/E vann, TIP5p vann og CO_2 ble mest sannsynlig begrenset av kinteikk ved lav temperatur, og termodynamikk ved høy temperatur. Monte carlo metoder skal ikke være begrenset av kinetikk, og dette kan derfor forklare noe av den ufysiske oppførselen. Selv om noen trender ble observert, ga simuleringene totalt sett lite data. Dette skyldes ufysisk oppførsel flere steder i systemet, og er mest sannsynlig fordi det ble utført for få monte carlo sykler. Ved å øke antall monte carlo cycler kan man muligens få kvantitative data.

Preface

This master thesis have been carried out at Norwegian University of Science and Technology (NTNU) at the Department of Material Science and Engineering as a part of my master's degree in chemical engineering and biotechnology. The master thesis has been supervised by Assoc. Professor Sondre K. Schnell and Phd candidate Jacob Hadler-Jacobsen at NTNU. The idea behind the project is credited to Assoc Professor Sondre K. Schnell.

Acknowledgements
First and foremost i would like to thank my supervisor Sondre K. Schnell for his guidance throughout this thesis. His knowledge regarding computational chemistry has been of great value to me. Secondly, i would like to thank my co-supervisor Jacob Hadler-Jacobsen. Your guidance during this thesis has been excellent.

I would also like to thank my parents, who have been both supportive and critical (when needed) towards my decisions and priorities. Lastly i would like to thank Trine for her support during these months.

Table of Contents

List of Tables

List of Figures

Nomenclature

Abbreviations

MD	Molecular dynamics
MC	Monte Carlo
MCMC	Markov Chain Monte Calro
MH	Metropolis-Hasting
CFMC	Continuous fractional Monte Carlo
LJ	Lennard-Jones potential

Mathematical symbols

Δ G	Gibbs free energy	kJol^{-1}
Δ H	Enthalpy	kJmol^{-1}
T	Temperature	K
P	Pressure	Pa
R	Ideal gas constant	J$(molK)^{-1}$
V	Volume of the system	Å^3
m_{host}	Mass of host particles	g
m_{ads}	Mass of adsorbed particles	g
r	radius	Å
N	Number of atoms	
μ_{ads}	Chemical potential	
N_{host}	number of atoms in the framework	
μ	old state	
ν	new state	
P_μ	Probability to find the system in state μ	
P_ν	Probability to find the system in state ν	
P($\mu \rightarrow \nu$)	Probability to perform a transition from state μ to ν	
$\hat{s}$	Position of all atoms in the system	
h	Planck constant	
k_b	Boltzmann constant	
U^ν	Energy of the system when in the new state ν	
U^μ	Energy of the system when in the old state μ	
V_μ	Volume of system at old state μ	
V_ν	Volume of system at new state ν	
λ	Scaling parameter for the CFMC algorithm	
ϵ	Well-depth LJ potential	
σ	Collision diameter LJ potential	
u_{Coul}	Electrostatic energy as coulombic potential	
ϵ_0	Permitivity of free space	
q_i	Charge of particle i	
q_j	Charge of particle j	
E($\hat{r}, \hat{p}$)	Energy of a molecular system as a function of momentum and length	
$\kappa(P)$	kinetic energy as a function of momentum	
m_i	mass of particle i	
3N-N_c	Degrees of freedom for a molecular system	
t	time	
F_{xi}	Force on particle i in direction x	
U	Molecular energy	

$u_b(r)$	Energy change of a molecule due to bond stretching
$u_\theta(\theta)$	Energy change of a molecule due to bending of bond
$u_\phi(\phi)$	Energy change of a molecule due to torsion
$u_{nb}(r)$	Energy change of a molecule due to non-bonded interactions
k	Spring constant
V_n	Amplitude height
n	Number of minimas in energy
ϕ	Phase factor
$\hat{n}$	
L	All directions in a supercell
α	Gaussian curves
$\hat{k}$	Reciprocal vector
$S(\hat{k})$	Structure factor
r_off	End of switching function
r_{on}	Start of switching function

Chapter 1

Introduction

1.1 Motivation

The energy demand increases as more countries worldwide prosper. Simultaneously the pollution from extracting and consuming the energy increases the global warming in prevalence and serenity. The worlds energy consumption in 2015 was 110358 TWh and are expected to increase further for the years to come [1]. 87 % of the energy consumed was obtained from coal, oil and natural gas. There is no doubt that a paradigm shift is needed in the production and consumption of energy, and the need for better materials for CO_2 capture are huge. Adsorption hcan be used to separate CO_2 from gas mixtures [2]. At the same time, development and utilization of batteries have potential to solve the CO_2 emission problems from today's coal and fossil fuel driven energy production. In 2004 an interesting discovery was made, Geim et al. discovered the first two dimensional material, Graphene [3]. Two dimensional materials are generally of interest due to their physical and electrical properties compared to bulk materials [4]. Several two dimensional materials have been discovered since then, and in 2011 Naguib et al. discovered the first MXenes [5]. MXenes are synthesized from a family of compounds, and as of 2017, 20 different MXenes has been synthesized with dozen of more predicted to be stable [6]. Of all MXenes, Ti_2C has the highest specific surface area of all MXenes synthesized, which makes it an interesitng material regarding adsorption [7].

Since its discovery, MXenes has gained a lot of attention form the scientific community. Especially the application as a cathode material in lithium and magnesium batteries is profound [8, 9]. There have also been investigations of MXenes as a CO_2 capture material, with promising results [10]. Several studies has shown promising results regarding intercalation of small ions, as well as large organic molecules [11, 12, 13, 14]. These adsorptive properties is most likely due to the uneven layered nature of multilayered MXenes [15].

Although there have been a lot of theoretical studies on MXenes, few investigate multilayered MXenes [16].

1.2 Approach

The object of this thesis is to study adsorption in multilayered bulk Ti_2C MXene with O and F as termination groups. This will be done by molecular simulations, Monte Carlo methods and Molecular dynamics in the osmotic ensemble. The adsorbents consists of two water models, TIP5p and SPC/E, CO_2 and diglyme. The simulation of the water models is done to investigate the hydrophilic properties of MXenes. The simulations CO_2 in MXenes is done to investigate MXenes as a CO_2 capture and storage material, whereas Diglyme is simulated to investigate MXenes properties in electronic storage devices (Diglyme is often used as an electrolyte in batteries). These simulations will be performed in RASPA, which is a software package developed to performe simulations on flexible molecule frameworks.

Chapter 2

Theory

2.1 MXenes

MXenes are a family of 2D transition metal carbides and/or carbonitrides [7]. The chemical composition of the MXene is $M_{n+1}X_nT_x$, where M refers to an early transition metal, X is Carbon or Nitrogen, and T_X is a surface termination group which must be present for the MXene to be stable. Non surface-terminated MXenes has not yet been synthesized, and are predicted to be thermodynamically unstable [17].

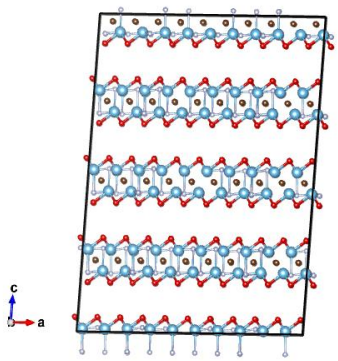

Figure 2.1: This figure shows the composition of a bulk mxene with chemical composition Ti_2C. This MXene are surface terminated by Oxygen and Fluor. The brown atoms represent Carbon, the blue represent Titanium, the red Oxygen and the white Fluor.

Figure 2.1 shows the atomic layers of a bulk mxene. Here, the brown atoms represent Car-

bon, and the blue atoms represent Titanium. The red and the white atoms show the surface termination groups and represent Oxygen and Fluro respectively. The interlayer forces in an MXene is a combination of two forces, hydrogen forces between the surface termination groups, and weak Van der Waals forces between the layers [15]. The c-lattice parameter of MXenes also show that there is an uneven spacing between the layers. The surface termination groups of MXenes makes it possible to alter electronic properties properties. Bare MXene layers are metallic, whereas when terminated they become semiconducting [7]. This termination also impart hydrophilicity to the MXene [6, 7]. The hydrophilic nature makes it possible for water to intercalate between the MXene layers spontaneous at ambient conditions [11].

2.1.1 Adsorptive properties

The high specific surface area of MXenes, and especially of the M_2X_1 materials (M_2X_1 MXenes are showed to have the highest specific surface area of all MXenes) are of great interest regarding adsorption [7]. There have been several reports of intercalation of atoms, molecules and ions into MXene layers [11, 12, 13, 14]. This includes Lead, H_2, CO_2, water, and large organic molecules. Intercalation between MXene layers have shown a significant increase in the c-lattice parameter between the layers [11]. This increase intuitively weaken the interaction between the layers. Due to the stacikng of many layered MXenes, which has shown a big variation in the c-lattice parameter between the layers, it is possible to intercalate large organic molecules between the MXene layers.

2.2 Adsorption

Adsorption of atoms and/or molecules are typically divided into two segments, chemical adsorption and physical adsorption [18]. The chemical adsorption is an irreversible process where a chemical bonding occurs between the adsorbate and the adsorbents. This is typically a slow process, which requires some activation energy to occur. Physical adsorption is the result of Van der Waals forces between the adsorbates and the adsorbents. This is a quick, reversible reaction that occurs at lower temperature than chemical adsorption. The extent of adsorption on a solid is dependent on several thermodynamic factor. Since adsorption generally is an exothermic process, it should increase with decreasing temperature. The description of thermodynamic properties of adsorption can be done in several ways. In this thesis, two classification methods shall be used, Heat of adsorption and adsorption isotherms.

2.2.1 Thermodynamics

For adsorption at a constant pressure, the Gibbs free energy can be expressed as

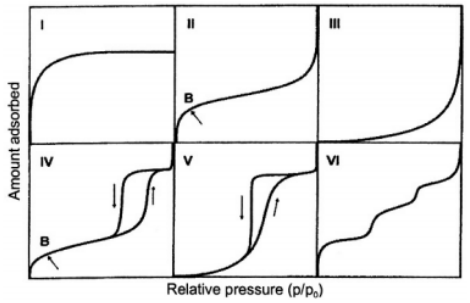

Figure 2.2: The 6 different types of adsorption isotherms.

$$\Delta G = \Delta H - T\Delta S \tag{2.1}$$

where ΔH is the enthalpy, T is the temperature and ΔS is the entropy [19]. For an exothermic process, the value of ΔH is negative, whereas ΔH is positive for an endothermic process. ΔG either increases or decreases for an exothermic or endothermic process respectively. This has three implications for equation 2.1.

1. ΔH or ΔS are negative, and the term involving ΔS dominates the expression
2. ΔH is negative and ΔS is Positive
3. ΔH or ΔS are negative and the term involving ΔH dominates the expression

Case 1 is an entropy driven adsorption, case 2 gives an exothermic process with increased disorder, whereas case 3 is an enthalpy driven adsorption.

Adsorption isotherms

An adsorption isotherm represents the amount adsorbed in a solid as a function of equilibrium pressure [20]. This is used to gain insight of the amount adsorbed in a solid. It gives an idea of how the pressure affects the adsorption, and what the adsorbed amounts are at different pressures. The typical adsorption isotherm shows an decrease in adsorption as the temperature increases, due to that adsorption generally are exothermic. The shape of the different adsorption isotherms can tell what type of adsorption is occurring inside the framework. There are 6 different types of adsorption isotherms classified by IUPAC [21].

Figure 2.2 represents the adsorption isotherms used for classification. The isotherm obtained from an experiment or simulation is classified with respect to their shape [22]. A type I adsorption isotherm represents an Langmuir isotherm. It is represented with a

convergence towards an adsorbed amount even at higher pressure. Type II and III represent adsorption on macroporous adsorbents with a weak interaction between adsorbates-adsorbents. Types IV and V represents mono and multilayer adsorption, with capillary condensation, and a type VI isotherm represents an adsorption isotherm with more than one step, which is typical for multilayered 2 dimensional materials [23]

Heat of adsorption

The heat of adsorption gives an indication of how strong the interaction is between the adsorbate and the adsorbent, and are used to distinguish between physical and chemical adsorption [24]. Heat of adsorption values below 50 kJ/mol indicates physical adsorption, whereas heat of adsorption values above 50 kJ/mole indicates chemical adsorption. This is because chemical adsorption involve the formation and breakage of chemical bonds, which involves higher energies than physical adsorption. There are several ways to measure the Heat of adsorption, but the most popular is the isosteric heat of adsorption [20]. The isosteric heat of adsorption are obtained from adsorption isotherms, at a constant loading, and calculated from the Clausius-Clapeyron equation [25].

$$\frac{\delta lnP}{\delta T} = \frac{q_{st}}{RT^2} \tag{2.2}$$

Equation 2.2 shows the Clausius-Clapeyron equation on differential form. Here, P is the pressure at constant loading, T is the temperature, q_{st} is the isosteric heat of adsorption, and R is the gas constant. The isosteric heat of adsorption for a system can be obtained by plotting $\ln$P against T^{-1} for various loadings. q_st are a positive quantity, meaning that negative values for heat of adsorption is nonphysical.

2.3 Molecular simulations

Molecular simulations is a wide variety of computational methods used for the simulation of molecular systems [26]. Although many methods exist, Molecular Dynamics simulations and Monte Carlo methods are two very powerful methods that's applicable for a wide variety of molecular systems. These two methods will be used to study adsorption in MXenes in this thesis.

2.3.1 ensemble

Statistical mechanics distinguish between two sets of states, microstates and macrostate. Macrostates represents macroscopic properties of the system, such as temperature and

pressure. Microstates refer to the state of the system by refering to the position and momenta of each particle inside the system. Simulations on a many-body thermodynamic system involves taking time-averages over the phase-space curve of the system [27]. The phase-space is the combination of all of the microscopic states in the system [28]. To describe a microscopic state of the system, 6N variables is needed [27]. Each of the N atoms in the system has three positions and three momenta. There are eight ensambles to perform both MD and MC simulations in [27]. These simulations have different applications for the properties calculated of the system. In this thesis, the osmotic ensamble will be elaborated further.

Osmotic ensamble calculations

It is well established that the osmotic ensamble is the right ensamble to simulate adsorption in a flexible framework [29, 30, 31, 32]. The osmotic ensamble has a fixed chemical potential for the adsorption molecule (μ_{ads}), a fixed number of atoms in the framework (N_{host}), constant temperature and constant pressure [33]. $\mu_{ads}N_{host}Tp$ ensamble describes a system open to adsorbate exchange with a resrvoire with fixed chemical potential, which is in contact with a thermal reservoir with fixed temperature, and a pressure reservoir with fixed pressure. Since the ensamble has a fixed pressure the volume of the host-framework will adjust to hold the pressure constant [27].

2.3.2 Markov Chain Monte Carlo methods

A Markov Chain Monte Carlo (MCMC) method is a numerical method to estimate average properties of systems with a large number of accessible states [27]. Markov chain refers to a chain of states where the probability of each state depends on the previous state [34]. Here, the generated state could be either a new state, or the same old state. In esscense, an MCMC method, if run long enough, generates a set of equilibriated probability distributions. For the method to generate the right probability distribution, some requirements must be fulfilled. One of these is the condition of ergodicity, which is the requirement that it should be possible for the markov process to access any state of the system from any other state of the system. Another requirement to generate the right distribution is the condition of detailed balance. This requirement states that the probability flux between each state is zero. In mathematical terms the condition of detailed balance is written as

$$p_\mu P(\mu \to \nu) = p_\nu P(\nu \to \mu) \tag{2.3}$$

Equation 2.3 shows the condition of detailed balance [34]. Here, p_μ defines the probability to find the system in state μ, and $P(\mu \to \nu)$ is the probability of a transition form state μ to state ν.

$$\frac{P(\mu \to \nu)}{P(\nu \to \nu)} = \frac{p_\nu}{p_\mu} = e^{-\beta(E_\nu - E_\mu)} \tag{2.4}$$

Equation 2.4 shows the tansition probability. Here, $\beta = (k_b T)^{-1}$, and k_b is the Boltzmann constant. E_ν and E_μ is the energy of state ν and state μ. By fulfilling the condition of ergodicity, the condition of detailed balance, and having a transition probability on the form shown in equation 2.4, the right probability distribution for the system is generated.

The most famous MCMC algorithm is the one of Metropolis et al. called the Metropolis-Hasting algorithm [35]. This algorithm applies all of the requirements mentioned above, and has an acceptance probability defined as

$$P(\mu \to \nu) = \min(1, \frac{P_\mu}{P_\nu}) \tag{2.5}$$

Equation 2.5 shows the acceptance probability in the MH algorithm. It states that, for a transition from state μ to state ν to be accepted, a random number generated from a uniform distribution must be between 1 and the value of $\frac{p_\mu}{p_\nu}$.

Several different algorithms exist for MCMC methods, and simulations in different ensambles are possible [34]. When simulating adsorption in flexible frameworks, as mentioned earlier, the Osmotic ensamble is a natural ensamble to choose. There are four distinct changes MCMC methods tries to perform on the system in the osmotic ensambel [33].

1. Configurational change of particles
    - Bond stretching
    - Bond bending
    - Bond torsion
2. Change of the volume and/or size of the system
3. Creation of an adsorbate particle at a random place in the system
4. Deletion of a random adsorption particle in the system

The equilibriated probability distribution for the osmotic ensamble has the form [27]

$$P(\hat{s}, V, N_{ads}) \propto \frac{1}{\Lambda_{host}^{3N_{host}} N_{host}!} \frac{V^N e^{\beta \mu_{ads} N_{ads}}}{\Lambda_{ads}^{3N_{ads}} N_{ads}!} e^{-\beta(U(\hat{s}:\hat{h}) + pV)} \tag{2.6}$$

Equation 2.6 shows the probability distribution for simulations in the osmotic ensemble. Here, $\Lambda_{\text{host}} = h/\sqrt{2\pi m_{\text{host}} k_b T}$ and $\Lambda_{\text{ads}} = h/\sqrt{2\pi m_{\text{ads}} k_b T}$. $\hat{s}$ is the position of all atoms. From equation 2.6 the probability to perform the four system changes can be written as

Configurational change of particles

$$\frac{p_\mu}{p_\nu} = e^{-\beta[U^\nu(s^{\hat{N}};\hat{h}) - U^\mu(s^{\hat{N}};\hat{h})]} \tag{2.7}$$

Where β represents $(k_bT)^{-1}$, and k_b is the Boltzmann constant. U_ν for the new state, and $U_m u$ is the energy for the old state.

Insertion to framework

$$\frac{p_\mu}{p_\nu} = \frac{Ve^{\beta\mu_{ads}}}{\Lambda^3_{ads}(N_{ads}+1)} e^{-\beta[U_n(\hat{s}^{N+1};\hat{h}) - U_o(\hat{s}^N;\hat{h})]} \tag{2.8}$$

Where V is the volume of the unit-cell, μ_{ads} is the chemical potential of adsorbates and N_{ads} is the number of adsorbate molecules,

Deletion from framework

$$\frac{p_\mu}{P_\nu} = \frac{\Lambda^3_{ads}N_{ads}}{Ve^{\beta\mu_a ds}} e^{-\beta[U_\nu(\hat{s}^{N-1}) - U_\mu(\hat{s}^N;\hat{h})]} \tag{2.9}$$

Change of volume of the unit-cell

$$\frac{p_\mu}{p_\nu} = \frac{V_\nu}{V_\mu} e^{-\beta p(V_\nu - V_\mu)} e^{-\beta[U_\nu(\hat{s}^N;\hat{h}) - U_\nu(\hat{s}^N;\hat{h})]} \tag{2.10}$$

Where V_ν is the new volume, V_μ is the old volume, N is the number of framework atoms and p is the pressure. To perform one of the moves mentioned above on the system, the acceptance rule presented in equation 2.5 must be fulfilled.

2.3.3 Continuous fractional Monte Carlo

At high densities, insertion and deletion of molecules in a flexible framework become vanishingly low [36]. To overcome these difficulties, Shi et al. proposed a Monte Carlo Scheme called Continuous Fractional Monte Carlo (CFMC) [36, 37]. The CFMC method relaxes a physical system by fading in (or out) the interaction between fractional and whole

molecules. It does so by using an scaling in Lennard-Jones potential and electrostatic potential, with a parameter λ [27].

$$u_{LJ}(r) = \lambda 4\epsilon \left[\frac{1}{[\frac{1}{2}(1-\lambda)^2 + \frac{r}{\sigma}^6]^2} - \frac{1}{[\frac{1}{2}(1-\lambda)^2 + \frac{r}{\sigma}^6]} \right] \tag{2.11}$$

Equation 2.11 shows the scaling of Lennard-Jones potential in the CFMC scheme. The scaling of electrostatic interactions takes the form

$$u_{Coul} = \lambda^5 \frac{1}{4\pi\epsilon_0} \frac{q_i q_j}{r} \tag{2.12}$$

The scaling in equation 2.11 and 2.12 makes the system slowly "inflate" and "deflate" molecules in the framework like a balloon. In addition to the system moves presented in equation 2.7-2.10, an adittional change in λ is possible. This change is made according to $\lambda(\nu) = \lambda(\mu) + \Delta\lambda$. Here, the $\Delta\lambda$ is chosen uniformly between $-\Delta\lambda^{max}$ and $\Delta\lambda^{max}$. For the change $\lambda(\mu \to \nu)$, there are three potential outcomes.

1. λ remains between 0 and 1
   The inter molecular energy of the fractional molecule, $\lambda(\mu \to \nu)$ changes with a Metropolis like acceptance ratio (equation 2.5).

   $$\frac{p_\mu}{p_\nu} = \min(1, \mathrm{e}^{-\beta[U_\nu - U_\mu] + \eta(\lambda(\nu)) - \eta(\lambda(\mu))}) \tag{2.13}$$

   No real change to the system is performed, only λ and the inter molecular energies change.

2. λ becomes larger than 1
   The current fractional molecule is made fully present in the framework, and a new fractional particle is randomly inserted.

3. λ is less than 0
   The current fractional molecule is deleted from the framework, and a new fractional molecule is added.

Adaption to the osmotic ensamble have been made, such that the implementation to this ensamble is possible [36].

2.3.4 Molecular dynamics

It is possible to consider a classical many body molecular system as mechanical [26]. By doing this, it is possible to apply the general laws of mechanics to calculate velocities,

forces and energy for this system. The energy is generally split in two terms, kinetic energy, $\kappa(P)$ and the potential energy $U(r)$.

$$E(\hat{r}, \hat{p}) = U(\hat{r}) + \kappa(\hat{p}) \tag{2.14}$$

The instantaneous temperature is related through the systems kinetic energy via the momentum

$$\kappa = \sum_{i=1}^{N} \frac{|\hat{p}_i|}{m_i} = \frac{k_b T}{2}(3N - N_c) \tag{2.15}$$

where $3N - N_c$ represents the degrees of freedom for the system, and $\hat{p_i}$ is the momentum vector. k_b represents the boltzmann constant. The information about the interaction of the molecules are represented in the potential energy term. These interactions are described earlier (equation 2.25 and 2.21). When simulating a molecular system, the interactions arising from the potential function can be used to describe the forces in an equation of motion, and the entire time-evolution of the system can be calculated.

These principles are applied in Molecular Dynamics simulations, which evolves around the integration of Newton's laws of motion [26]. By solving the differential equation embodied in newtons second law, it produces a trajectory which specifies how the positions and the velocities of the system vary with time.

$$\frac{d^2\hat{r}}{dt^2} = \frac{F_{x_i}}{m_i} \tag{2.16}$$

Equation 2.16 shows the differential equation obtaind from Newtons second law. Here x denotes the position of direction, t is the time, F_{x_i} is the force that acts upon the particle in the x-direction, and m_i is the mass of the particle. By solving this equation, the trajectory is created.

2.3.5 Hybrid Monte Carlo method

The hybrid Monte Carlo method was first proposed by Duane et al [38]. This Monte Carlo scheme uses MD to generate MC trial moves [39]. This is an advantage because the constraints on what defines a good MC move are not as strict as for a good MD move. Especially regarding the time step MD uses to integrate newtons laws of motion. Using hybrid MC, it is possible to take a time step that is too long for MD, as long as the algorithm is time reversible and area preserving, and use this as a criterion for the acceptance of an MC move. In hybrid MC, every trial move chooses the particle velocities at random from the Maxwell-Boltzmann distribution.

2.4 Molecular force fields

Molecular force fields are a set of parameters used to define the interactions inside a molecules, as well as interactions between molecules [39]. These parameters makes it able to treat a molecular system as mechanical, thus making it possible to simulate using either MCMC, MD or a combination thereof. The intermolecular interactions usually consist of bond stretching, angle bending and torsion. The interaction between molecules, so-called non-bonded interaction are Van der Waals interactions and electrostatic interactions.

$$U = \sum_{bonds} u_b(l) + \sum_{bends} u_\theta(\theta) + \sum_{torsions} u_\phi(\phi) + \sum_{non-bonded} u_{nb}(r) \quad (2.17)$$

Equation 2.17 shows the molecular energy as a Taylor expansion in bonds, bends, torsions etc [27]. The change in bond, bend and torsion are self parameters, and only change the molecular energy. The non-bonded interactions describe the interaction between the molecules, and are Van der Waals force and electrostatic interactions [26]. These interactions are usually modelled as Lennard-Jones potential and Coulombic interactions.

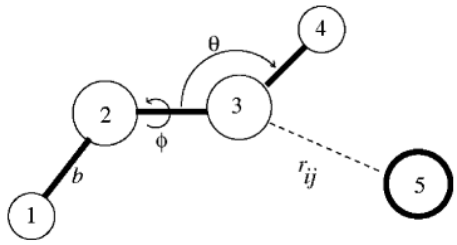

Figure 2.3: Inter- and intra molecular forces described by a force field.

Figure 2.3 illustrates how the different changes inside a molecule apply, as well as the non-bonded interactions between molecules

2.4.1 Bond-, bend- and torsion potential

The easiest way to simulate the bond stretching and bending inside a molecule is with use of harmonic motions [26].

$$u_{bond}(l) = \frac{k}{2}(l - l_0)^2 \quad (2.18)$$

Equation 2.18 shows the bond stretching inside a molecule modelled as a harmonic motion.

Here k is a constant, l_0 is the initial bond position and l is the offset bond position. The angle bending is also described the same way.

$$u_{bond}(\theta) = \frac{k}{2}(\theta - \theta_0)^2 \tag{2.19}$$

Equation 2.19 shows the angle bending inside a molecule modelled as a harmonic motion. Here θ_0 is the initial position of the bond, and θ is the offset position after the bond has been bent x degrees. Bothe the equation 2.18 and 2.19 can also be modelled with the use of hooks law.

The torsion inside a molecule describes the energy change when a twist around a central atom occur [26]. It describe how atoms move around an axis, and interact with the electron cloud of other atoms in the molecule. This can be modelled as a periodic motion.

$$u(\omega) = \frac{V_n}{2}[1 + \cos(n\omega - \gamma)] \tag{2.20}$$

Equation 2.20 describes the energy change of a molecule due to torsion. V_n is the amplitude height, n describes the number of minimas in the energy, and γ is the phase factor.

Several terms can be added to equation 2.17 and equation 2.20 to more accurately simulate the bond stretching/angle bending and torsion inside a molecule, or even express hydrogen bonding. In reality this is a trade-off between realistic behaviour and computational power, and a complicated computational-heavy model is usually not an advantage.

2.4.2 Electrostatic interactions

Electrostatic interactions are a type of non-bonded interactions which occurs due to charge differences between particles [26]. These interactions are described by a Coulombic potential, which decays proportionally to r^{-1} [27]. In a system with several particles, the electrostatic potential energy between particles with point charge q_i at the position $\hat{r_i}$ is given by

$$U(r) = \frac{1}{4\pi\epsilon_0} \sum_{i<j} \frac{q_i q_j}{|\hat{r_{ij}}|} \tag{2.21}$$

Equation 2.21 shows how the electrostatic interactions typically are modelled in a force field. ϵ_0 is the permitivity of free space. For a system consisting of only a small number of molecules, equation 2.21 is easy to evaluate. However, in molecular mechanics it is usually of interest to compute macroscopic properties of the system, whilst the number of particles is as low as possible. By applying Periodic boundary conditions (PBC) to the

system, it is possible to study a infinate system with a finite number of particles [26]. PBC replicates the unit cell through space. Thus, if a particle is in one side of the unit cell, it reappears on the other side of the unit cell. When applying PBC to a system, it is usual to also apply the minimum image convention of the electrostatic potential. For a periodic system, a particle should be able to "see" all the other particles in the system.

$$U(r) = \sum_{j,n}^{'} \frac{q_j}{|\hat{r_{ij}} + \hat{n}L|} \tag{2.22}$$

Equation 2.22 shows the coulombic potential when th minimum image convention is applied [39]. The prime in the summation indicates that the sum is over all periodic images $\hat{n}$ except when $j = i$ if $\hat{n} = 0$. L represents the supercell. $L = [|x|, |y|, |z|$. For a periodic system, equation 2.22 is conditionally convergent and cannot be used to calculate the electrostatic energy. To be able to solve equation 2.22, numerical methods must be applied. One such method is Ewald summation [40]. Ewald summation splits the summation to two series, which converges faster [27].

$$\frac{1}{r} = \frac{\text{erf}\,(\alpha r)}{r} + \frac{\text{erfc}\,(\alpha r)}{r} \tag{2.23}$$

Equation 2.23 deals with the rapid variation of $\frac{1}{r}$ at small r, and the slow decay of $\frac{1}{r}$ at long r. α represents the gaussian curves.

The Ewald method assumes that each point charge is surrounded by an neutralizing charge distribution of equal magnitude, but opposite sign [26]. Equation 2.23 shows that the charges has been splitted to a dual summation, the charges, plus the neutralising distribution. This is done to convert the conditionally convergent sum from equation 2.22, to a convergent sum. By applying the Ewald summation for a periodic system on the Coulombic interaction, the ewald expression for the Coulombic energy reads[1]

$$\begin{aligned}\frac{U}{V} = \frac{1}{2V\epsilon_0} \sum_{k\neq 0} \frac{\exp\,(-\frac{k^2}{4\alpha})}{k^2} S(\hat{k})S(-\hat{k}) \\ + \frac{1}{2} \sum_{i,j} \sum_{\hat{n}}^{'} \frac{q_i q_j\, \text{erfc}\,(\alpha|\hat{r_{ij}} + \hat{n}|)}{|\hat{r_{ij}} - \hat{n}|} \\ - \sum_i \frac{2\alpha}{\sqrt{\pi}} q_i^2\end{aligned} \tag{2.24}$$

In equation 2.24, the first term represents a summation in the reciprocal space, where

[1] The complete derivation of this can be found in [39]

$\hat{k} = \frac{2\pi\hat{n}}{L}$, and is a reciprocal vector. α is the gaussian curves, and thus a lower α leads to a faster convergence. The second term represents the real space summation. This summation also contains the gaussian curve α, but in this term a higher α leads to faster convergence. It is therefor obvious that a balanced α must be chosen for the optimal convergence. The third term denotes the correction of the sum of the Gaussian functions in real space that interacts with itself, and must therefor be substracted.

2.4.3 Van der waals interaction

Van der Waals forces accounts for the charges that is not due to charge differences between particles [26]. These interactions are weaker than electrostatic interactions, and consists of both. At a long range, the interaction energy between two particles are zero, and at short range they diverge. The attraction between the molecules are due to dispersive forces, which occurs due to fluctuations in the electron clouds. The repulsive forces occurs when two particles are very close to eachother. When the particles get two close to eachother, same-spin electrons will overlap and cause a divergence in the potential energy of the particles. This is also known as the Pauli principle.

Van der Waals forces between molecules, and between framework and molecules, are usually modelled as a Lennard-Jones potential.

$$u^{vdw}(r) = 4\epsilon_{ij}\left[\left(\frac{\sigma_{ij}}{r}\right)^{12} - \left(\frac{\sigma_{ij}}{r}\right)^{6}\right] \tag{2.25}$$

Equation 2.25 shows the Van der Waals forces between particles as a Lennard-Jones potential. Here ϵ represents the well- depth, and σ represents the collision diameter [26]. r^{-12} represents the repulsive part, and r^{-6} the attractive part, thus, Lennard-Jones potential combines the Van der Waals forces and the Pauli repulsion.

The molecular parameters (ϵ and σ) used when calculating the LJ potential is usually defined as self-parameters, meaning that they are defined as interactions between equal molecules or atoms. To be able to compute the interaction between several different molecules, a mixing of these molecules must be performed. The Lorentz-Berthelot mixing rule is a way to do this [41].

$$\epsilon_{ij} = \sqrt{\epsilon_i \epsilon_j} \tag{2.26}$$

$$\sigma_{ij} = \frac{\sigma_i + \sigma_j}{2} \tag{2.27}$$

Equation 2.27 shows Lorentz-Berthelot mixing rule used to define the Lennard-Jones potential between different particles.

The realism on the simulations depends heavily on the long-range interactions, but they are also computational heavy. By assigning a cut-off to the LJ potential, which neglects the long range interactions after a certain distance, the computations can be made more efficient [42]. This is possible because the long tail on the LJ potential for large distances. For MC simulations, the potential can be truncated after the cutoff, and the resulting error in the potential is the are between the x-axis and the LJ potential [27]. For MD simulations on the other hand, a truncation of the potential leads to divergence in the forces, and other means must be considered. A typical way to deal with this is the use of a switching function, which forces the potential to go smoothly to zero at the cutoff. One of these switching functions was proposed by Steinbach et. al. [42].

$$u(r_{ij}) = \begin{cases} u(r_{ij}) & \text{if} \quad r_{ij} < r_{on} \\ u(r_{ij}) \frac{(r_{off}^2 - r^2)(r_{off}^2 + 2r^2 - 3r_{on})}{(r_{off}^2 - r_{on}^2)^3} & \text{if} \quad r_{on} \leq r_{ij} \leq r_{off} \\ 0 & \text{if} \quad r_{ij} > r_{off} \end{cases} \tag{2.28}$$

Equation 2.28 shows how the potential are switched during MD simulations. The switching term occurs when $r_{on} \leq r \leq r_{off}$. This is represented as a cubic function, which must satisfy $u(r_{on}) = 1$, $u(r_{off}) = 0$, $\frac{du}{dr}(r_{on}) = 0$ and $\frac{du}{dr}(r_{off}) = 0$, which gives a continuous potential energy and force. When considering a cut-off distance, it is required that the smallest perpendicular distance of the simulation cell is larger than twice the cut-off distance [27].

Chapter 3

Computational procedure

This chapter addresses the simulations performed in this thesis. Algorithms, approximation methods, temperature- and pressure discretization will be elaborated. All simulations are implemented in RASPA, which is a molecular software package for simulation of adsorption and diffusion in flexible nanoporous materials [43].

The adsorbates simulated in the MXene frameworke are;

1. CO_2
2. SPC/E water model
3. TIP5p water model
4. Diglyme

3.1 Approximations

All of the components simulated share some settings regarding their approximation methods. All molecules have a spherical cut-off at 12.0 Å. At this length, all non-bonded interactions are neglected. During the MC cycles the potential are truncated at 12.0 Å, whereas during the MD cycles the potential are shifted by the switching function presented in equation 2.28, and are 0 at 12.0 Å. The electrostatic interactions are approximated by the Ewald summation (equation 2.24), with a precision of $10^{-}5$. The time steps for the different adsorbates are presented in table 3.1. The framework is simulated as flexible, with a defined probability to perform a volume change of unit cell. A probability to attempt a hybrid MC

move using MD in the NVE-ensamble is also defined. MD integrates Newton's equation of motion for the whole system, and accepts or rejects this move with the standard MC rule showed in equation 2.5. These two probabilities are defined relative to each other, and scaled to be accepted 50 % of the times.

Table 3.1: Monte Carlo cycles and time step for Molecular dynamics simulations.

Molecule	Number of Cycles	Number of Initialization cycles	Time step
CO_2	70000	10000	0.00025
SPCE water	70000	10000	0.0005
TIP5p water	70000	10000	0.0005
Diglyme	100000	10000	0.00025

3.2 Initialization

The initialization of the system is done to ensure the desired temperature in an equilibrium configuration [27]. First in the initialization process, N molecules are inserted in to the box at random positions, as long as no overlaps occur. For a solid framework, inaccessible pockets may be present. These boxes are blocked of, and no molecule will be inserted in these. Then, an NVT MC simulation is performed to rapidly equilibrium. After this is done, all the velocities are assigned to the molecules from the Maxwell-Boltzmann distribution at the desired average temperature. The total momentum of the system is set to zero to avoid centre of mass drift of the system.

3.3 Molecular force fields

The creation of all molecular force fields used in the calculation are presented below. All the force fields uses the same type of inter and intra molecular energy terms, provided in equation 2.18, 2.19, 2.20, 2.21 and 2.25. The mixing of these parameters are calculated with the use of Lorenz-Berthelot mixing rule, provided in equation 2.27

3.3.1 Mxene framework

The MXene framework are created in accordance to the force field provided by Muckly et al. [44]. It has chemical compostion Ti_2C, with O and F as termination groups. The termination groups has stoichiometry $O_2F_{0.8835}$, to ensure that the framework has a net charge of 0.

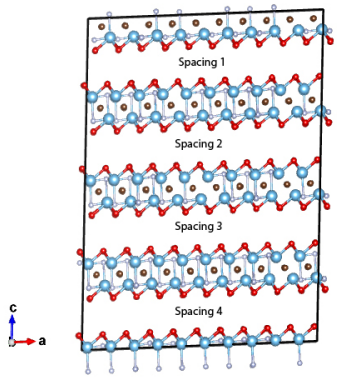

Figure 3.1: Unit cell with the different MXene layers. The brown atoms represents Carbon, the blue atoms represents Titan, the red atoms Oxygen, and the white atoms fluor. PBC is applied, so in reality this represents 4 mxene layers. The spacing between the layers are indicated as they are presented in the results section

Figure 3.1 shows the MXene framework simulated. The spacings indicated in the figure are presented in the result section, and gathered by using Vesta [45]

Table 3.2: Parameters used to define the force field for $Ti_2C(O_x, F_x)$.

Atom	$\mathbf{q}_i$ [e]	ϵ [K]	σ [Å]
Ti	1.53189	78.18	3.166
C	1.24356	78.18	3.166
F	-0.7	78.18	3.5532
O	-0.9	78.18	3.5532

Table 3.2 shows the parameters used to define the MXene force field.

3.3.2 Water models

Creating water-like models for use in molecular simulations has proven to be challenging [46]. There are several reasons for this. One is that in comperance to other liquids, water presents a number of anomalies [47]. In solid state, the phase diagram is complex, with fifteen different solid structures [46]. This being said, some models manage to replicate water behaviour at ambient conditions. In this work, the SPC/E and TIP5p water models are being used to simulate water adsorption in the MXene framework.

SPC/E

The extended simple point charge (SPC/E) water model is modelled as a rigid isosceles triangle, with charges on each of the three atoms [48]. These charges are three point charges, one for each atom in the molecule. It is defined with long range Lennard-Jones interactions (see equation 2.25). In the SPC/E water model, the Lennard-Jones parameters are self-parameters with interaction based on Oxygen-Oxygen repulsion/attraction.

Table 3.3: Parameters used to define the force field for the SPC/E water model.

Atom	$\mathbf{q}_i$ [e]	ϵ [K]	σ [Å]
O	-0.8476	78.18	3.166
H	0.4238	0	0
Force field	**Bond length** [Å]	**Bond angle** [deg]	
SPC/E	O-H=1.00	O-H-O = 109.47	

Table 3.3 shows the parameters used to define the force field for the SPC/E water model

TIP5p

The TIP5p water model is modelled as a 5 site water molecule, where two of the sites simulates the lone electron pair of oxygen in the water molecule [49]. The oxygen atom possesses no charge, but has a Lennard-Jones potential working between the oxygen atoms of the water molecules. The electrostatic interactions are calculated for every charged site on the molecule.

Table 3.4: Parameters used to define the electrostatic interactions and the LJ potential for the TIP5p water model. L denotes the charge used to describe the lone pair in a water molecule. All parameters are self-parameters, and their interactions are calculated by Lorentz-Berthelot mixing rule (equation 2.27).

Atom	$\mathbf{q}_i$ [e]	ϵ [K]	σ [Å]
O	0	78.18	3.097
H	0.241	0	0
L	-0.241	0	0
Force Field	**Bond length**	**Bond angle**	
TIP5p	O-H = 0.9572	H-O-H = 104.52	
	O-L = 0.7	L-O-L = 109.47	

Table 3.4 shows the parameters used to define the force field for the TIP5p water model.

3.3.3 CO_2

The CO_2 molecule is made in accordance to the TraPPE force fields [50]. The atoms in the molecule is modelled as three LJ sites, to approximate the overlap and the dispersion forces. At these sites, point charges are placed in the center. The bond lengths between the atoms are fixed at their experimental value.

Table 3.5: Parameters used to define the electrostatic interactions and the LJ potential for the CO_2 molecule.

Atom	$\mathbf{q}_i$ [e]	ϵ [k]	σ [Å]
C	0.7	27.0	2.80
O	-0.35	79.0	3.43
Force Field	**Bond length** [Å]	**Bond angle** [deg]	
CO_2	C-O = 1.16	O-C-O = 180	

Table 3.5 shows the parameters used to define the force field for the TIP5p water model.

3.3.4 Diglyme

The diglyme molecule is created in accordance with the force field provided by Barbosa et al [51]. It uses harmonic motions for the tratment of bond stretching and angle bending (see equation 2.18 and 2.19), and a periodic motion for the treatment of torisons (equation 2.20). The Lorentz-Berthelot mixing rules are used to calculate the interaction between the atoms. The intramolecular forces that ar separated by one or two bonds are set to 0, whereas the intramolecular forces separated by three bonds are scaled to 0.5 and $\frac{5}{6}$ for the LJ potential and the electrostatic interactions respectively. The Parameters used to describe the LJ potential, as well as the electrostatic interactions, are presented in table 3.6.

Table 3.6 shows the parameters used to define the force field for the Diglyme molecule

Table 3.6: Parameters used to define the electrostatic interactions and the LJ potential for the diglyme molecule.

Atom	$\mathbf{q}_i$	ϵ [K]	σ [Å]
C_{g1}	0.179006	49.547	3.502
C_{g2}	0.185194	49.547	3.502
C_{g3}	0.454852	49.547	3.502
O_{g1}	-0.472073	76.992	3.09
O_{g2}	-0.64592	76.992	3.09
H_{g1}	0.016637	7.111	2.545
H_{g2}	0.010291	7.111	2.545
H_{g3}	-0.047256	7.111	2.545
Bond			**Bond length** [Å]
C-C			1.535
C-O			1.439
C-H			1.093
Bond			**Bond angle** [deg]
C-O-C			112.45
H-C-H			109.55
H-C-O			108.82
C-C-O			108.42
C-C-H			110.07

Chapter 4

Results

This chapter addresses the results obtained in this thesis. The main focus will be the adsorption isotherms for the different molecules simulated in the framework, the heat of adsorption obtained from this adsorption, and the variation of the C-lattice parameter for the bulk MXene framework. Regarding the adsorption isotherm, the general isotherm will be presented, as well as the adsorbed amount at 100 000 Pa (1 bar) and 500 000 Pa (5 bar). The heat of adsorption presented are gathered from fluctuations in energy and density from the different molecules simulated. This adsorption is simulated in RASPA, in the osmotic ensemble with a Hybrid MC-MD simulation. This is done with the probability distribution presented in equation 2.6 . For the adsorption and deletion of molecules, Equation 2.8 and equation 2.9 is used for the acceptance or rejection. The Volume change is decided according to equation 2.10.

All molecules are simulated at 6 different temperatures;

1. 273 K
2. 293 K
3. 313 K
4. 333 K
5. 353 K
6. 373 K

The C-lattice parameter is presented to get an idea of the movement inside the bulk MXene, and how the C-lattice parameter between the different layers in the MXene vary as a

function of the pressure (which correlates best with the variation of the C-lattice length). The volume changes of the unit cell gives no significant data, thus they will not be presented.

4.1 Adsorption isotherms

In this section, the adsorption isotherms of each of the species (if an adsorption occurred) will be presented. The adsorption is presented on weight basis, relative to the weight of the framework.

4.1.1 CO_2

The CO_2 force field is created in accordance with the parameter given in table 3.5, and are simulated as a rigid molecule. The pressures simulated are from 1 Pa, up to 500 000 Pa (5 bar) with a logarithmic spacing between the pressure points.

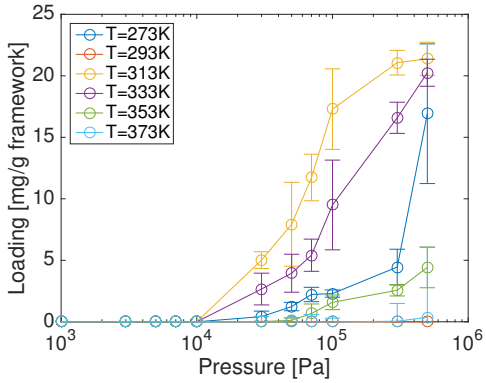

Figure 4.1: Adsorption isotherms for CO_2

Figure 4.1 shows the adsorption isotherms of CO_2 at the various temperatures. The adsorption at 313 K, 333 K and 273 K starts at 10000 Pa, whereas 353 K and 373 K starts at 50000 Pa and 100000 Pa respectively. the adsorbed amount is highest at 313 K for all pressures, where it seems to converge to 21.38 $\pm$ 1.35 mg/g framework. None of the other temperatures shows sign of convergence. At 293 K the framework did not exhibit any adsorption, and the adsorption at 373 K is insignificant compared to the uncertainty calculated. This implies that the isotherms are somewhat unphysical.

Table 4.1 shows the amount adsorbed in the framework at 100 000 Pa and 500 000 Pa. The uncertainties are calculated by RASPA. Note that the framework does not adsorb any molecules at 293 K, and that for 373 K the uncertainty is larger than the adsorbed amount.

Table 4.1: Amounts CO_2 adsorbed in the MXene framework at the different temperatures and pressures.

Pressure [Pa]	**Temperature** [K]	**Amount adsorbed** [mg/g framework]
100000	273	2.295 ± 0.295
	293	0
	313	17.3 ± 3.27
	333	9.5 ± 3.65
	353	1.58 ± 0.597
	373	0.0007 ± 0.0028
500000	273	16.92 ± 5.68
	293	0
	313	21.38 ± 1.35
	333	20.25 ± 1.10
	353	4.43 ± 1.66
	373	0.37 ± 0.75

4.1.2 SPC/E water model

The SPC/E water model force field is created with accordance to the parameters given in table 3.3. It is simulated from 0.1 Pa to 500 000 Pa with a logarithmic spacing between each point.

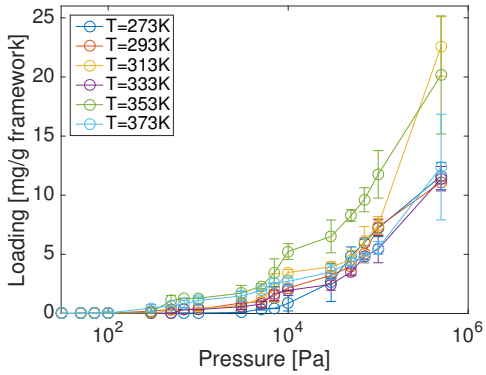

Figure 4.2: Adsorption isotherms for SPC/E water model

Figure 4.2 shows the adsorption isotherms of the SPC/E water model as a function of pressure. The adsorbed amounts is generally very low at low pressures, and increases as the pressure increases. The framework adsorbes most SPC/E water at a temperature of 313 K at 500 000 Pa, with 353 K just below. The isotherms shows no correlation of the adsorbtion being temperature dependent, meaning that there is no clear trend in either higher or lower temperature adsorbes the most SPC/E water. The adsorbed amount of SPC/E water at 100 000 Pa and 500 000 Pa is presented in the table 4.2.

Table 4.2: Amounts of SPC/E adsorbed in the MXene framework at the different temperatures and pressures.

Pressure [Pa]	**Temperature** [K]	**Amount adsorbed** [mg/g framework]
100000	273	7.21 ± 0.71
	293	7.32 ± 0.67
	313	7.45 ± 0.74
	333	5.43 ± 1.14
	353	11.76 ± 2.01
	373	5.55 ± 0.55
500000	273	11.62 ± 1.15
	293	11.09 ± 0.12
	313	11.09 ± 0.12
	333	11.4 ± 1.15
	353	20.17 ± 4.99
	373	12.38 ± 4.47

Table 4.2 shows the amount of SPC/E water adsorbed at 100 000 Pa and 500 000 Pa respectively. The low amount adsorbed is somewhat nonphysical, and the uncertainties presented should most likely be bigger.

4.1.3 TIP5p water model

The TIP5p water model force field is created in accordance with the parameters presented in table 3.4. The molecule is simulated as a rigid molecule, with a pressure discretization ranging from 0.1 Pa to 500 000 Pa with a logarithmic spacing between each point.

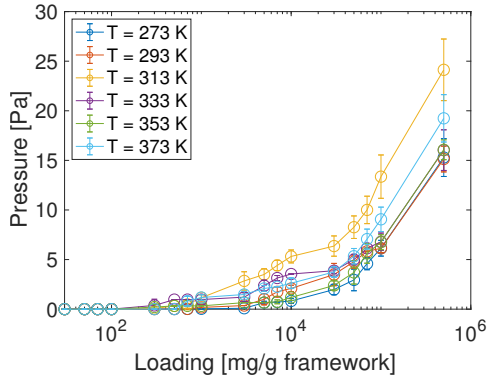

Figure 4.3: Adsorption isotherms for TIP5p water model

Figure 4.3 shows the adsorption isotherms for the adsorption of the TIP5p water molecule. Here, the adsorption shows the same general trend as for SPC/E water with an increase in adsorbed amount as a function of pressure. The temperature with the highest adsorbed amount is 313 K, which also is the same as it was for the SPC/E water model. The adsorption does not show any signs of convergence. A convergence indicates that the maximum adsorbed amount is reached. Table 4.3 shows the adsorbed amount at 100 000 Pa and 500 000 Pa.

Table 4.3: Amounts of TIP5p adsorbed in the MXene framework at the different temperatures and pressures.

Pressure [Pa]	**Temperature** [K]	**Amount adsorbed** [mg/g framework]
100000	273	6.14 ± 0.79
	293	6.14 ± 0.42
	313	13.36 ± 2.19
	333	6.79 ± 0.88
	353	6.75 ± 0.75
	373	9.06 ± 1.23
500000	273	15.12 ± 1.25
	293	13.57 ± 0.11
	313	22.54 ± 5.20
	333	15.36 ± 1.36
	353	22.4 ± 1.69
	373	22.39 ± 1.02

Table 4.3 show the adsorbed amount for all temperatures at 100 000 Pa and 500 000 Pa respectively. The low amount adsorbed is somewhat nonphysical, and the uncertainty should most likely be bigger.

4.1.4 Diglyme

Diglyme was not adsorbed in the framework at any temperature, thus no adsorption isotherm were obtained.

4.2 Heat of adsorption

The isosteric heat of adsorption is calculated using Calusius-Clapeyron's equation, shown in equation 2.2. The calculation is performed on the same adsorbed amounts for the isotherms, at different pressures. The presented plot is a mean isosteric heat of adsorption calculated between the different adsorption isotherms.

4.2.1 CO_2

The isosteric heat of adsoption for CO_2 is calculated from the adsorption isotherms at 273 K, 313 K and 333 K. This is due to the low adsorption amount from the two other isotherms.

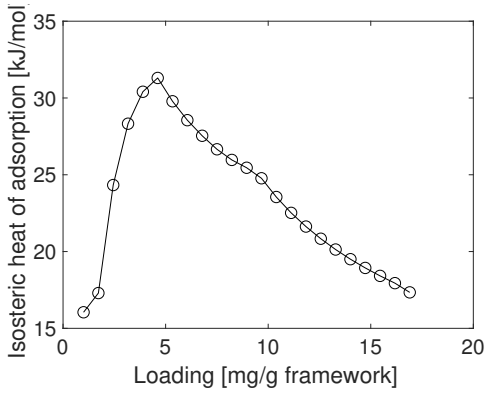

Figure 4.4: Isosteric heat of adsorption for CO_2 at various loadings.

Figure 4.4 shows the isosteric heat of adsorption for CO_2 at different loadings. A sharp increase in the isososteric heat of adsorption is obesrved at lower loadings, until it reaches a loading of 5 mg/g framework, then it starts to decrease and reaches a final value of 17.21 kJ/mol

4.2.2 SPC/E water model

The isosteric heat of adsorption for the SPC/E water model is calculated from all of the adsorption isotherms at different loadings. The values appear to fluctuate quite a bit, with isosteric heat of adsorption ranging from 15 to 2 kJ/mol.

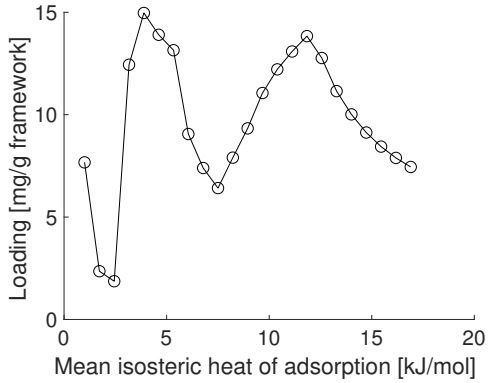

Figure 4.5: Isosteric heat of adsorption for SPC/E water at various loadings

Figure 4.5 shows the isosteric heat of adsorption for SPC/E water at different loadings.

4.2.3 TIP5p water model

The isosteric heat of adsorption for the TIP5p water model is calculated from all the adsorption isotherms at different loadings

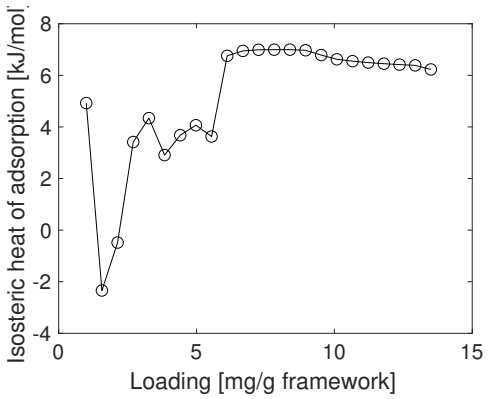

Figure 4.6: Isosteric heat of adsorption for TIP5p water at various loadings

Figure 4.6 shows the isosteric heat of adsorption for TIP5p water at different loadings. The isosteric heat of adsorption are generally very low. It also shows negative values, which is nonphysical due to the isosteric heat of adsorption being a positive quantity

4.3 C-lattice parameter

By looking at the C-lattice parameters (the spacing normal to the surface of the layers in the bulk MXene) it is possible to get an understanding of how the layers vary dependent on pressure and/or adsorption. The different spaces presented are shown in figure 3.1. In this section the C-lattice parameter as a function of pressure will be shown. The pressure where the adsorbtion starts are indicated with a black vertical line, and the mean layer spacing in between the layers in the bulk MXene are shown.

4.3.1 CO_2

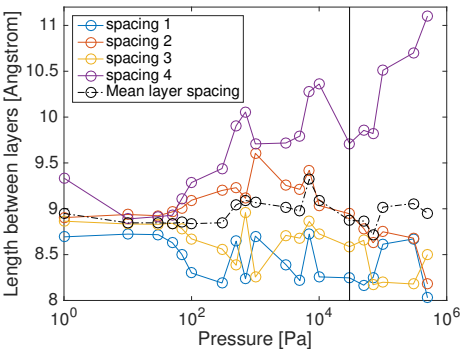

(a) C-lattice parameter as a function of pressure at 273 K

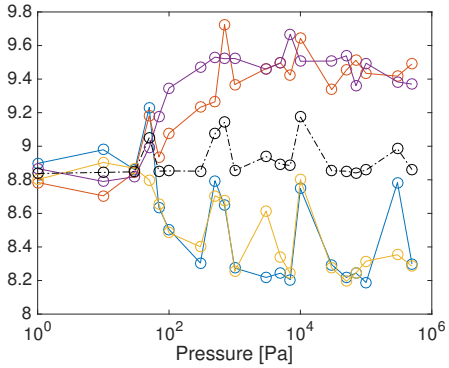

(b) C-lattice parameter as a function of pressure at 293 K

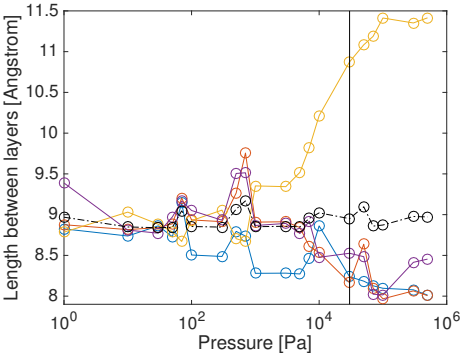

(c) C-lattice parameter as a function of pressure at 313 K

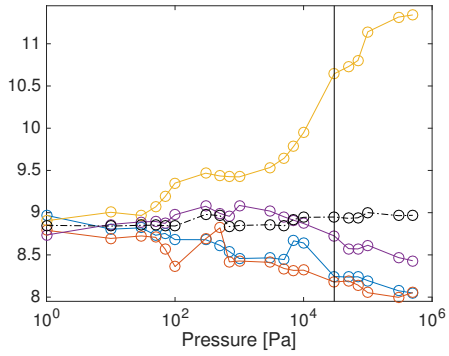

(d) C-lattice parameter as a function of pressure at 333 K

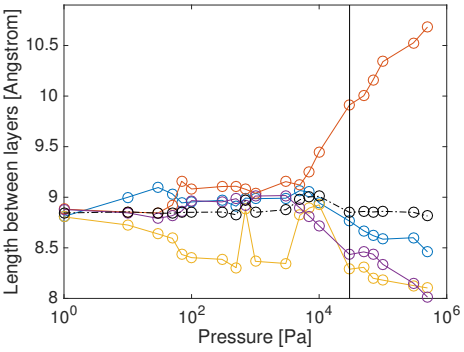

(e) C-lattice parameter as a function of pressure at 353 K

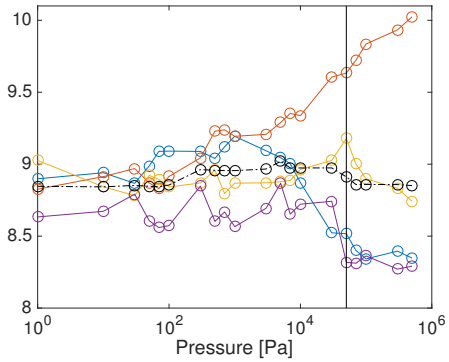

(f) C-lattice parameter as a function of pressure at 373 K

Figure 4.7: C-lattice parameters [Å] for CO_2 at at all temperatures as a function of pressure. The black vertical line indicates at which pressure the adsorption started. If no black vertical line is presented, there was no adsorbtion. The mean value of all the C-lattice parameters are also presented. The lines between each point is only included to guide the eyes.

Figure 4.7 shows how the c-lattice length vary as a function of pressure for the different MXene layers at different temperatures. The adsorption occurs between the layers with the greatest c-lattice length. At the start of the simulation, the inter-layer distance for the bulk MXene is around the same value for all the layers. As pressure increases, the inter-layer distance increases for some layers, and decreases for others. The adsorption does not start until two layers has a much greater spacing than the other, and which layers that is varies. Although there are a great variation of the spacing between the layers across the pressure span, the mean layer spacing seems to be somewhat constant for all the temperatures, independent of adsorbed amount. An important remark to make is that the MXene layers did not adsorb any CO_2 at 293 K, shown in figure 4.7b. This graph clearly shows that four layers obtained a greater spacing than the other layers, whereas for all the other temperatures only two layers gained a greater spacing than the others. The inter-layer distance at the point of adsorption between all layers is presented in the table below.

Table 4.4: Spacing between the layers at the pressure where the adsorption began for all temperatures for CO_2.

Temperature and Pressure [K] [Pa]	**Spacing**	**C-lattice length** [Å]
273, 30 000	Spacing 1	8.25
	Spacing 2	8.94
	Spacing 3	8.59
	Spacing 4	9.71
293, no adsorption	-	-
313, 10 000	Spacing 1	8.86
	Spacing 2	8.53
	Spacing 3	10.21
	Spacing 4	8.48
333, 30 000	Spacing 1	8.24
	Spacing 2	8.18
	Spacing 3	10.65
	Spacing 4	8.72
353, 30 0000	Spacing 1	8.76
	Spacing 2	9.91
	Spacing 3	8.29
	Spacing 4	8.43
373, 50 000	Spacing 1	8.52
	Spacing 2	9.63
	Spacing 3	9.18
	Spacing 4	8.32

4.3.2 SPC/E water model

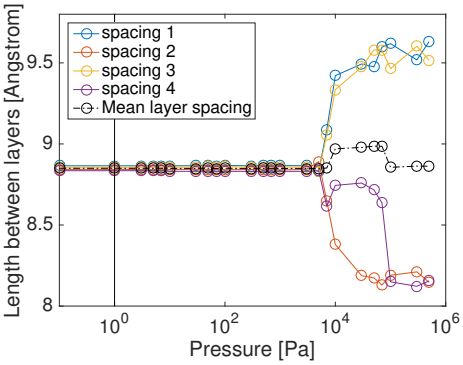

(a) C-lattice parameter as a function of pressure at 273 K

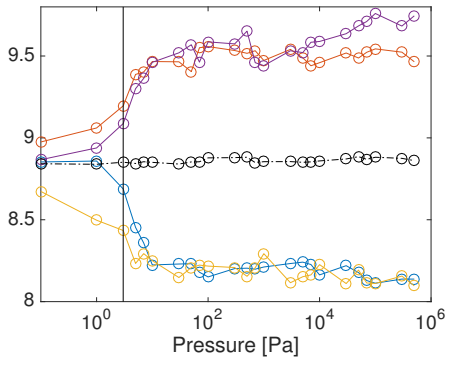

(b) C-lattice parameter as a function of pressure at 293 K

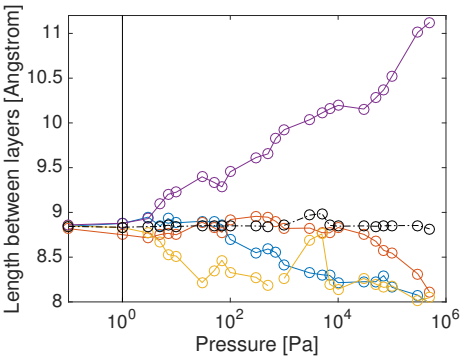

(c) C-lattice parameter as a function of pressure at 313 K

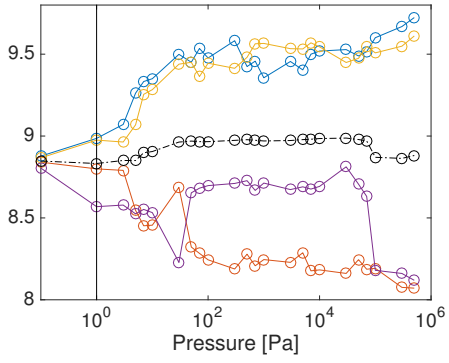

(d) C-lattice parameter as a function of pressure at 333 K

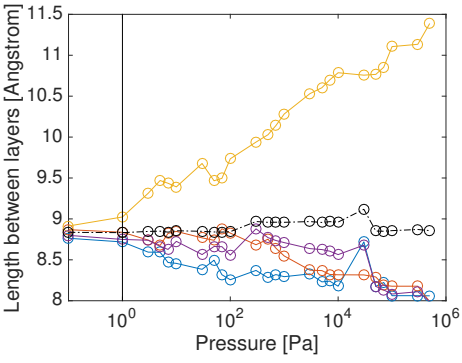

(e) C-lattice parameter as a function of pressure at 353 K

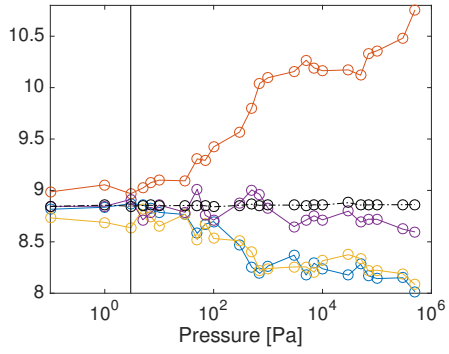

(f) C-lattice parameter as a function of pressure at 373 K

Figure 4.8: C-lattice parameters [Å] for SPC/E water model at at all temperatures as a function of pressure. The black vertical line indicates at which pressure the adsorption started. The mean value of all the C-lattice parameters are also presented. The lines between each point is only to guide the eyes.

Figure 4.8 shows the variation between the layers in the bulk MXene as a function of the pressure applied, for the SPC/E water model. The vertical black line represents the pressure where the adsorption first occurred. At 273 K, shown in figure 4.8a, the layers are extreamly stable, until around 10^4 Pa. For all the other layers the differene in spacing between the layers appear to become greater after the loading starts. Figure 4.8a, 4.8b and figure 4.8d, two spacings are greater than the other two, compared to the other temperatures. This clearly indicates that the adsorption happens in these two spacings, instead of only one spacing as the other figures show. It also reveals that as long as the adsorption happens in several spacings, the spacing between the layers where the adsorption occured has a maximum distance around 9.5 to 9.6 Å, whereas for the figures where the adsorption happened between two layers, this spacing becomes larger than this. Regarding the mean layer spacing, which is the mean spacing between all the layers, it is somewhat constant independent of pressure and loading for all temperatures. Table 4.6 shows the different spacings between the layers at the point of loading.

Table 4.5: Spacing between the layers at the pressure where the adsorption began for all temperatures.

Temperature and Pressure [K] [Pa]	**Spacing**	**C-lattice length** [Å]
273, 1	Spacing 1	8.87
	Spacing 2	8.84
	Spacing 3	8.86
	Spacing 4	8.84
293, 3	Spacing 1	8.86
	Spacing 2	9.1
	Spacing 3	8.5
	Spacing 4	8.94
313, 1	Spacing 1	8.88
	Spacing 2	8.75
	Spacing 3	8.83
	Spacing 4	8.88
333, 1	Spacing 1	8.99
	Spacing 2	8.8
	Spacing 3	8.98
	Spacing 4	8.57
353, 1	Spacing 1	8.72
	Spacing 2	8.84
	Spacing 3	9.02
	Spacing 4	8.75
373, 3	Spacing 1	8.84
	Spacing 2	9.06
	Spacing 3	8.69
	Spacing 4	8.85

4.3.3 TIP5p water model

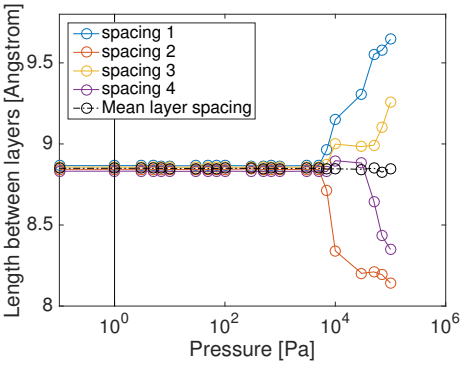

(a) C-lattice parameter as a function of pressure at 273 K

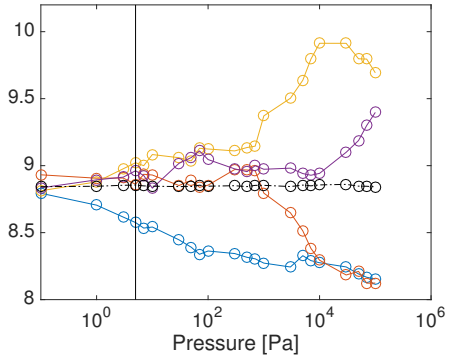

(b) C-lattice parameter as a function of pressure at 293 K

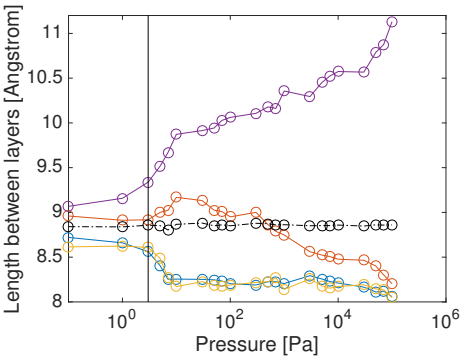

(c) C-lattice parameter as a function of pressure at 313 K

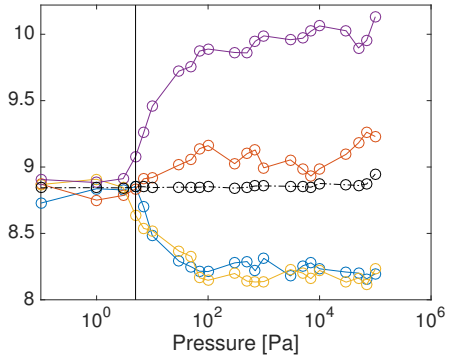

(d) C-lattice parameter as a function of pressure at 333 K

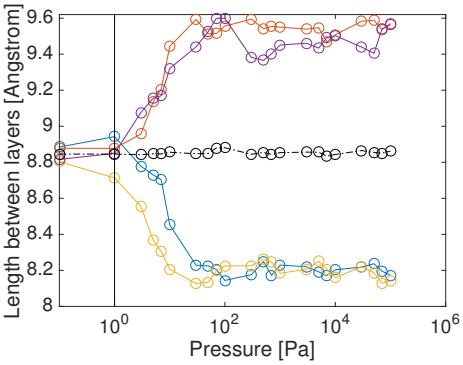

(e) C-lattice parameter as a function of pressure at 353 K

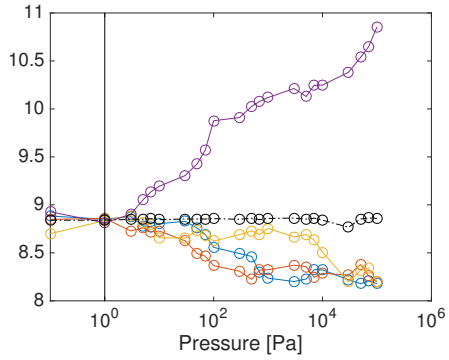

(f) C-lattice parameter as a function of pressure at 373 K

Figure 4.9: C-lattice parameters [Å] for TIP5p water model at at all temperatures as a function of pressure. The black vertical line indicates at which pressure the adsorption started. The mean value of all the C-lattice parameters are also presented. The lines between each point is only to guide the eyes.

Figure 4.9 shows the variation in the spacing between the layers in the bulk MXene as a function of pressure for the TIP5p water model. The pressure where the adsorption started is indicated with a black vertical line. Figure 4.9a shows that the spacing was close to constant for the bulk MXene at 273 K until it reached a pressure of 10^4 Pa, at this pressure the loading starts to become significant. Here, it is clear that the adsorption occurred between four layers at 353 K in figure 4.9e. The spacing has a maximum value of 9.33 Å where the adsorption occured. The mean layer spacing (indicated with a black dotted line) are close to constant throughout the pressure span.

Table 4.6: Spacing between the layers at the pressure where the adsorption began for all temperatures.

Temperature and Pressure [K] [Pa]	**Spacing**	**C-lattice length** [Å]
273, 1	Spacing 1	8.87
	Spacing 2	8.84
	Spacing 3	8.86
	Spacing 4	8.83
293, 5	Spacing 1	8.86
	Spacing 2	8.86
	Spacing 3	9.02
	Spacing 4	8.96
313, 1	Spacing 1	8.56
	Spacing 2	8.92
	Spacing 3	8.61
	Spacing 4	9.33
333, 5	Spacing 1	8.7
	Spacing 2	8.91
	Spacing 3	8.53
	Spacing 4	9.26
353, 1	Spacing 1	8.8.94
	Spacing 2	8.88
	Spacing 3	8.71
	Spacing 4	8.8.85
373, 3	Spacing 1	8.88
	Spacing 2	8.73
	Spacing 3	8.89
	Spacing 4	8.90

Chapter 5

Discussion

This chapter address's to discuss the results obtained in this thesis. Firstly, the adsorption isotherms will be elaborated, and the effects that might cause them to behave in the way shown will be elaborated. Secondly, the heat of adsorption will be discussed. Lastly, the c-lattice length. A further discussion will follow, which tries to combine all of these topics.

5.1 Adsorption isotherms

The adsorption isotherms for the different species simulated presented in figure 4.1, 4.2 and 4.3 appears to adsorb the most molecules at 313 K, and the adsorption decreases for lower and higher temperatures (with some deviations from this general trend, like CO_2 at 293 K). Liu et al found that for methane adsorbed in MXene, the adsorption rose with temperature. They concluded that with an increase in temperature implied an increase in adsorption capacity. It is clear that this conclusion cannot be drawn for any of the species adsorbed in the framework. The adsorption isotherm for TIP5p water model (seen in figure 4.3, the SPC/E water model (seen in figure 4.2) the adsorption of CO_2 (seen in figure 4.1) has adsorbed the most molecules at 313 K, whereas the Diglyme molecule were not adsorbed in the framework for any temperature or pressure.

5.1.1 Shape of the isotherms

The different shapes of the isotherms were presented in section 2.2.1. Looking at the adsorption isotherm for CO_2, especially at 313 K, it shows a clear convergence towards an adsorbed amount. This implies that the shape of the isotherm correlates with a type

5 adsorption isotherm. It is a reasonable assumption that the other adsorption isotherms for CO_2, will take the for higher loadings. The reason for this is that the only difference between these isotherms is the temperature, which implies that there is no physical reason for the isotherms to take another shape. For the SPC/E water model and the TIP5p water model, which were presented in figure 4.2 and 4.3, the isotherm shape correlate some with an type 3 adsorption isotherm. It is expected that these two water models undergo the same adsorption type, due to the similarity of the models (they simulate the same molecule, even though some parameters are different). The difference in shape of the adsorption isotherms for CO_2, SPC/E water and TIP5p water are probably due to that CO_2 has adsorbed close to its maximum amount at 313 K (which is indicated by the convergence towards a loading amount), whereas SPC/E and TIP5p are able to adsorb more molecules at higher pressures. Regarding the shape of the isotherms, CO_2 shows a different type of isotherm than the two water models. This is probably due to that CO_2 has adsorbed close to its maximum amount between the layers where the adsorption occurred, whereas the two water models are able to adsorb more. Considering the framework simulated is a bulk MXene, there are several more spacing to intercalate molecules in. After a layer has adsorbed its maximum possible molecules, it is clear that it will start to intercalate molecules between the other layers in the MXene. Hence, this would imply that the adsorption isotherm would take the shape of a type 6 adsorption isotherm. The results obtained in this thesis does not provide evidence for this. A reason for this might be that the pressures simulated was not high enough to fill the layers, and thus the filling of other layers were not energetically favorable. Another reason, which is probably more valid, is that the volume of the unit-cell were close to constant throughout the simulations (except for 273 K for SPC/E water and TIP5p water). A constant volume unit-cell has limits regarding adsorption due to the limited movement of the layers. This is also non physical, due to the internal layer movement of a bulk MXene would imply that there would be a significant change in the volume of the whole MXene upon intercalation (significant in the Angstorm scale).

5.1.2 Adsorbed amounts

The adsorbed amount of the different molecules in the framework were presented in table 4.1 for CO_2, table 4.2 for SPC/E water, and table 4.3 for TIP5p water. The amount adsorbed are generally very low compared to existing literature. Due to the hydrophilic nature of MXene, water is known to spontaneous intercalate between the MXene layers at ambient conditions and ambient humidity. Considering this, the adsorbed amount at 100 000 Pa were expected to be a lot higher. In fact, the presented adsorbed amounts of the water model are somewhat nonphysical compared to what would be expected from the existing literature.

Combining the low adsorbed amounts with the isotherms for CO_2, which showed no adsorption at 293 K, and an insignificant adsorption at 373 K (due to the high uncertainty relative to the adsorbed amount), substantiate the assertion of the simulations showing nonphysical behaviour. There is no reason in the physics that the framework should adsorb moleculeas at every pressure except at 293 K.

5.1.3 Diglyme

Diglyme molecules were not adsorbed in the framework at any pressure, thus no adsorption isotherm is presented. Diglyme is a much bigger molecule than the other simulated molecules, with a total of 23 atoms. This makes it a much harder molecule to adsorb. Especially considering the volume evolution was close to constant throughout the simulations, there might not have been enough room for an adsorbance of this molecule to be energetically favorable.

5.1.4 General discussion

None of the adsorption isotherms gathered shows any general trend in the adsorption with respect to temperature. In fact, they appear to be somewhat random. Although, CO_2 shows that temperatures below and above 313 K adsorbes less (shown in figure 4.1). The reason for this can be found by considering the thermodynamics of the adsorption, or the kinetics of the adsorption. Looking at the adsorption isotherm for CO_2 from figure 4.1, the adsorption into the MXene framework decreases at temperatures below and above 313 K. This indicates that there is an activation energy barrier at lower temperatures (temperatures below 313 K) that the adsorption must overcome to be energetically favorable. This barrier is inversely proportional to the temperature, thus the energy barrier increases as the temperature decreases. Considering the higher temperature (temperatures above 313 K) adsorption, thermodynamic considerations must be taken into account. Even though the energy barrier decreases as the temperature increases, the spontanity of the reaction (the gibbs free energy) from equation **??** increases as the temperature increases. This makes the entropy term dominate the expression. Kinetics restricting the adsorption at low temperatures imply that too few MCMC cycles were performed. MCMC methods require equilibriated systems to sample from the right probability distribution, thus it should not be restricted by kinetics. This is substantiated by the low amount and high uncertainty for adsorption of CO_2 at 373 K, which is nonphysical. Also, the fact that no molecules were adsorbed at 293 K imply this. There is no reason in the physical reason that adsorption should occur at all other temperatures than 293 K. This reason is also valid for the SPC/E water, and the TIP5p water, which shows no correlation in adsorbed amount at the different temperatures.

5.2 Heat of adsorption

The heat of adsorption calculated by RASPA (presented in the appendix) shows huge uncertainties and are insignificant. These huge uncertainties imply that the system was not at equilibrium when the simulations were performed. The isosteric heat of adsorbtion is presented in figure 4.4 for CO_2, figure 4.5 for SPC/E water and figure 4.6 for TIP5p water. All of these curves are below 50 kJ/mol, which implies that the adsorption is of physi-

cal character (physisorption). Even though this is the case, these graphs should be taken with a grain of salt. Especially considering the isosteric heat of adsorption for TIP5p water, shown in figure 4.6, which shows negative isosteric heat of adsorption. This is not physically possible, and substantiate that the simulations performed shows nonphysical behaviour. This is in agreement with the heat of adsorption calculated by RASPA, which show no significant result due to extremely high uncertainties.

5.3 C-lattice parameter

Insertion of a fractional molecule between two random layers in the framework, provided by the CFMC algorithm in section 2.3.3, causes these two layers to drift apart. This is due to repulsion between the adsorbate and the adsorbent. Figure 4.7 for CO_2, 4.8 for SPC/E water and 4.9 for TIP5p water shows the c-lattice parameter between the layers in the framework as a function of pressure. Looking at table 4.4, which shows the c-lattice parameter at the pressure where the loading first occurred for CO_2, it indicates that a minimum value of 9.71 Å is sufficient for the intercalation of atoms by the regular MCMC scheme (presented in section 2.3.2). For CO_2 it is a big spread in the c-lattice parameter at the pressure where the loading first occurred, but the loading amount also varies. Considering the big difference in loading at the first pressure where loading takes place for all the temperatures, it is reasonable to assume that the c-lattice parameter becomes larger for the lattices that had several molecules adsorbed. This is due to the repulsion between adsorbed molecules and the framework. The more adsorbed molecules, the more repulsion, and thus bigger difference in c-lattice parameter. The c-lattice parameter might also explain why the framework did not adsorb any molecules at 293 K for CO_2. Looking at figure 4.7b, which shows the variation of spacing between the layers at 293 K, it shows that two layers gained a bigger spacing than the other layers. Considering that the volume of the unit cell was close to unchanged during the whole simulation, which implies that there is a restriction of the space between the layers relative to each other, the maximum distance between the two layers at 293 K might not possibly become larger. For all of the other temperatures, the frameworks adsorbed molecules. Figure 4.7 clearly shows that the the space between two layers became larger than of the others.

Looking at the c-lattice parameter for the SPC/E water model shown in figure 4.8 and the TIP5p water model shown in figure 4.9, they adsorb molecules at a much lower pressure than CO_2, and with a much lower spacing between the layers. This is most likely because of the hydrophilic nature of MXenes. The plots that show four layers with a bigger spacing than others, as seen in figure 4.8a, 4.8b and 4.8d for SPC/E water, and figure 4.94.9a and 4.9e for TIP5p, adsorbs molecules between four layers, instead of just two as for the others. This indicates that the CFMC arlgorithm inserted a fractional molecule in one layer, which later was accepted and turned in to a regular molecule in the framework. Simultaneously, and adsorption from the MCMC scheme occured between two other layers. The spacing where adsorption happened between four layers, were close to equal, shown in table 4.6 and **??**.

Figure 4.8a and figure 4.9a shows the c-layer spacing for both of the water models at 273 K. It is clear that until the loading become of significant size, these lattice spacings are extremely stable. This indicates that a the framework was in a meta stable state at 273 K both for SPC/E as well as for TIP5p, which again implies that too few Monte Carlos cylces were used.

Regarding the diglyme atom, it had a constant c-lattice parameter between the layers throughout the simulations. This is due to that the CFMC algorithm was not implemented for Diglyme (Because of an error in the source code). Without an fractional molecule inserted, and no adsorption occurring, there is no external force to alter the c-lattice parameter between the layers. This is substantiated by the volume evolution, which were close to constant throughout the simulations.

5.4 Further discussion

There is several reasons from the obtained results that substantiate the assertion that the system simulated shows nonphysical behaviour. For one, no adsorption at 293 K for CO_2 and an insignificant adsorption at 373 K implies that too MCMC cycles were performed. In addition to this, the huge uncertainties in the heat of adsorption calculated by RASPA, as well as the isosteric heat of adsroption which were negative for some loading's of TIP5p water implies this. The close to constant volume throughout the simulations is also not ideal, as the system were simulated as flexible, thus the volume should vary. The consequence of performing an MCMC simulation with too few cycles is that the ensamble averaging is not done at the equilibriated probability distribution, and the simulations give insignificant and non physical result. A solution to this is obviously to simulate the system with a lot more cycles. This again leads to a longer simulation time, and the simulations performed in this thesis used around 400 000 CPU hours. Considering this, a system with fewer atoms should also be considered.

Chapter 6

Conclusion

The aim of this thesis were to study the adsorption of CO_2, water and Diglyme in a flexible MXene framework. The calculations performed are based on Monte Carlo methods and molecular dynamics simulations, and a combination thereof. These calculations were performed in RASPA. The MXene layers were shown to adsorb slightly more water than CO_2 at 5 Pa. This corresponds well with the existing literature, which shows that MXenes are hydrophilic, and should adsorb more water than CO_2. Still, the amounts of water and CO_2 adsorbed does not nearly correspond the predicted amounts. The effects in the isotherms shown in figure 4.1, 4.2 and 4.3 may be due to kinetics limiting the adsorbance at low temperatures, and thermodynamics limiting the adsorbance at higher temperatures. Monte Carlo simulations should not be constricted by kinetics. Even though the simulations started out on low pressures, with a small pressure discretization, this points towards that the simulations should be performed with more cycles. This is substantiated by some nonphysical results, as seen in figure 4.1 where no CO_2 were adsorbed at 293 K. Also, the heat of adsorption calculated by RASPA shows no significant results due to extremely large errors. The isosteric heat of adsorption shows that the adsorption of SPC/E water, TIP5p water and CO_2 are physical adsorption, with heat of adorption below 50 kJ/mol at all loading's. The isosteric heat of adsorption for TIP5p water are negative for some loading's, which is nonphysical, and substantiate that the simulations were performed with too few cycles. Considering the c-lattice parameters for SPC/E shown in figure 4.8, CO_2 shown in figure 4.7, and TIP5p shown in figure 4.9, move initially due to the CFMC algorithm, and the spot where the CFMC algorithm tries to insert a fractional molecule is where the adsorption is most likely to occur. Although an adsorption between several layers were also shown to be possible. these seem to move independent on loading, which implies that the pressure is the driving force behind the movement. Adsorption happened either between two layers or four layers for SPC/E water and TIP5p layer, and only between two layers for CO_2. The adsorption between more than two layers occur when two layer spacings have close to equal length, and the length of these two spacings is larger than for

the other spacings. The mean length of the c-lattice parameters are close to constant for all the frameworks at all temperatures. This implies that the volume are unchanged during the simulations, which were the case. The framework was simulated as flexible, and the volume should vary with the loading.

Diglyme was not adsorbed in the framework at all, which is most likely due to the volume being close to constant throughout the simulations, and there was simply not enough space present for adsorption of Diglyme, which is a much bigger molecule than CO_2 and the water models.

This leads to the final conclusion that RASPA did not yield the desired results for the simulations performed in this thesis. This is especially substantiated by the huge error in the heat of adsorption calculated by RASPA, the fact that the volume of the unit cell was close to constant throughout the simulations, and that the adsorption of atoms was restricted by kinetics at lower temperatures. The results could probably be improved by increased number of cycles, thus they would provide results of greater significance.

Bibliography

[1] International Energy Agency. *Key World Energy Statistics 2017*. 2017.

[2] Xiaochun Xu, Chunshan Song, John M. Andresen, Bruce G. Miller, and Alan W. Scaroni. Novel polyethylenimine-modified mesoporous molecular sieve of mcm-41 type as high-capacity adsorbent for co2 capture. *Energy Fuels*, 16(6):1463–1469, 2002.

[3] K. S. Novoselov, D. Jiang, F. Schedin, T. J. Booth, V. V. Khotkevich, S. V. Morozov, and A. K. Geim. Two-dimensional atomic crystals. *Proceedings of the National Academy of Sciences*, 102(30):10451–10453, 2005.

[4] Rebecca Cheung and Rui Zhang. Mechanical properties and applications of two-dimensional materials. In Pramoda Kumar Nayak, editor, *Two-dimensional Materials*, chapter 10. InTech, Rijeka, 2016.

[5] Naguib Michael, Kurtoglu Murat, Presser Volker, Lu Jun, Niu Junjie, Heon Min, Hultman Lars, Gogotsi Yury, and Barsoum Michel W. Two-dimensional nanocrystals produced by exfoliation of ti3alc2. *Advanced Materials*, 23(37):4248–4253.

[6] MR. Gogotsi Y Anasori, B. Lukatskaya. 2d metal carbides and nitrides (mxenes) for energy storage. 2017.

[7] Naguib Michael, Mochalin Vadym N., Barsoum Michel W., and Gogotsi Yury. 25th anniversary article: Mxenes: A new family of two-dimensional materials. *Advanced Materials*, 26(7):992–1005.

[8] Dequan Er, Junwen Li, Michael Naguib, Yury Gogotsi, and Vivek B. Shenoy. Ti3c2 mxene as a high capacity electrode material for metal (li, na, k, ca) ion batteries. *ACS Applied Materials & Interfaces*, 6(14):11173–11179, 2014. PMID: 24979179.

[9]

[10] Angel Morales-Garcia, Adrian Fernandez-Fernandez, Francesc Vines, and Francesc Illas. Co2 abatement using two-dimensional mxene carbides. *J. Mater. Chem. A*, 6:3381–3385, 2018.

[11] Naresh C. Osti, Michael Naguib, Alireza Ostadhossein, Yu Xie, Paul R. C. Kent, Boris Dyatkin, Gernot Rother, William T. Heller, Adri C. T. van Duin, Yury Gogotsi, and Eugene Mamontov. Effect of metal ion intercalation on the structure of mxene and water dynamics on its internal surfaces. *ACS Applied Materials & Interfaces*, 8(14):8859–8863, 2016. PMID: 27010763.

[12] Neng Li, Xingzhu Chen, Wee-Jun Ong, Douglas R. MacFarlane, Xiujian Zhao, Anthony K. Cheetham, and Chenghua Sun. Understanding of electrochemical mechanisms for co2 capture and conversion into hydrocarbon fuels in transition-metal carbides (mxenes). *ACS Nano*, 11(11):10825–10833, 2017. PMID: 28892617.

[13] Qianku Hu, Dandan Sun, Qinghua Wu, Haiyan Wang, Libo Wang, Baozhong Liu, Aiguo Zhou, and Julong He. Mxene: A new family of promising hydrogen storage medium. *The Journal of Physical Chemistry A*, 117(51):14253–14260, 2013. PMID: 24261885.

[14] Qiuming Peng, Jianxin Guo, Qingrui Zhang, Jianyong Xiang, Baozhong Liu, Aiguo Zhou, Riping Liu, and Yongjun Tian. Unique lead adsorption behavior of activated hydroxyl group in two-dimensional titanium carbide. *Journal of the American Chemical Society*, 136(11):4113–4116, 2014. PMID: 24588686.

[15] Hsiu-Wen Wang, Michael Naguib, Katharine Page, David J. Wesolowski, and Yury Gogotsi. Resolving the structure of ti3c2tx mxenes through multilevel structural modeling of the atomic pair distribution function. *Chemistry of Materials*, 28(1):349–359, 2016.

[16] Kurt D. Fredrickson, Babak Anasori, Zhi Wei Seh, Yury Gogotsi, and Aleksandra Vojvodic. Effects of applied potential and water intercalation on the surface chemistry of ti2c and mo2c mxenes. *The Journal of Physical Chemistry C*, 120(50):28432–28440, 2016.

[17] M. Gogotsi Y. Anasori, B. Lukatskaya. 2d metal carbides and nitrides (mxenes) for energy storage. *Nature reviews materials 2*, 2017.

[18] A Dabrowski. Adsorption — from theory to practice. *Advances in Colloid and Interface Science*, 93(1):135 – 224, 2001.

[19] Papita Saha and Shamik Chowdhury. Insight into adsorption thermodynamics. In Mizutani Tadashi, editor, *Thermodynamics*, chapter 16. InTech, Rijeka, 2011.

[20] Paul C. Hiemenz and Raj Rajagoplan. *Principles if Colloid and Surface Chemistry*. Taylor and Francis, 3rd edition, 1997.

[21] S. Brunauer. *The Adsorption of Gases and Vapors*, volume 1. Princeton University press, 1945.

[22] *Adsorption Isotherms*, pages 359–413. Springer US, Boston, MA, 2005.

[23] A. W. Adamson. *Physical Chemistry of Surfaces*. John Wiley, 1976.

[24] Santiago Builes, Stanley I. Sandler, and Ruichang Xiong. Isosteric heats of gas and liquid adsorption. *Langmuir*, 29(33):10416–10422, 2013. PMID: 23808559.

[25] Wedler Gerd. The theory of adsorption and catalysis. physical chemistry, a series of monographs. von a. clark. academic press, new york–london 1970 1. aufl., x, 418 s., geb. dm 19.50. *Angewandte Chemie*, 83(11):417–417.

[26] Andrew R. Leach. *Molecular modelling: Principles and applications*. Prentice Hall, 2 edition, 2001.

[27] David Dubbeldam, Ariana Torres-Knoop, and Krista S. Walton. On the inner workings of monte carlo codes. *Molecular Simulation*, 39(14-15):1253–1292, 2013.

[28] Ian Ford. *Statistical Physics; An Entropic Approach*. Wiley.

[29] R. Q. Snurr, A. T. Bell, and D. N. Theodorou. Hierarchical atomistic/lattice simulation approach for the prediction of adsorption thermodynamics of benzene in silicalite. *Journal of Physical Chemistry*, 98(19):5111–5119, 12 1994.

[30] J. SHEN and P. A. MONSON. A molecular model of adsorption in a dilute semiflexible porous network. *Molecular Physics*, 100(13):2031–2039, 2002.

[31] John K. Brennan and William G. Madden. Phase coexistence curves for off-lattice polymersolvent mixtures: Gibbs-ensemble simulations. *Macromolecules*, 35(7):2827–2834, 2002.

[32] Brian J. Banaszak, Roland Faller, and Juan J. de Pablo. Simulation of the effects of chain architecture on the sorption of ethylene in polyethylene. *The Journal of Chemical Physics*, 120(23):11304–11315, 2004.

[33] Ralph J. Wolf, Myung W. Lee, Ricardo C. Davis, Patrick J. Fay, and John R. Ray. Pressure-composition isotherms for palladium hydride. *Phys. Rev. B*, 48:12415–12418, Nov 1993.

[34] G. Newman, M. Barkema. *Monte Carlo methods in Statistical Physics*. A K Peters Nakin, 1999.

[35] Nicholas Metropolis, Arianna W. Rosenbluth, Marshall N. Rosenbluth, Augusta H. Teller, and Edward Teller. Equation of state calculations by fast computing machines. *The Journal of Chemical Physics*, 21(6):1087–1092, 1953.

[36] Wei Shi and Edward J. Maginn. Continuous fractional component monte carlo: an adaptive biasing method for open system atomistic simulations. *Journal of Chemical Theory and Computation*, 3(4):1451–1463, 2007. PMID: 26633216.

[37] Wei Shi and Edward J. Maginn. Improvement in molecule exchange efficiency in gibbs ensemble monte carlo: Development and implementation of the continuous fractional component move. *Journal of Computational Chemistry*, 29(15):2520–2530, 11 2008.

[38] Simon Duane, A.D. Kennedy, Brian J. Pendleton, and Duncan Roweth. Hybrid monte carlo. *Physics Letters B*, 195(2):216 – 222, 1987.

[39] Daan Frenkel and Berend Smit. *Understanding molecular simulation; From algorithms to applications*. Academic Pess, 1996.

[40] Ewald PP. Die berechnung optischer und elektrostatischer gitterpotentiale. *Annalen der Physik*, 369(3):253–287.

[41] Lorentz H. A. Ueber die anwendung des satzes vom virial in der kinetischen theorie der gase. *Annalen der Physik*, 248(1):127–136.

[42] Peter J. Steinbach and Bernard R. Brooks. New spherical-cutoff methods for long-range forces in macromolecular simulation. *Journal of Computational Chemistry*, 15(7):667–683, 7 1994.

[43] David Dubbeldam, Sofía Calero, Donald E. Ellis, and Randall Q. Snurr. Raspa: molecular simulation software for adsorption and diffusion in flexible nanoporous materials. *Molecular Simulation*, 42(2):81–101, 2016.

[44] Eric S. Muckley, Michael Naguib, Hsiu-Wen Wang, Lukas Vlcek, Naresh C. Osti, Robert L. Sacci, Xiahan Sang, Raymond R. Unocic, Yu Xie, Madhusudan Tyagi, Eugene Mamontov, Katharine L. Page, Paul R. C. Kent, Jagjit Nanda, and Ilia N. Ivanov. Multimodality of structural, electrical, and gravimetric responses of intercalated mxenes to water. *ACS Nano*, 11(11):11118–11126, 2017.

[45] K. Momma and F. Izumi. Vesta 3 for three-dimensional visualization of crystal, volumetric and morphology data. *J. Appl. Crytallogr.*, 44:1272–1276, 2011.

[46] C. Vega, J. L. F. Abascal, M. M. Conde, and J. L. Aragones. What ice can teach us about water interactions: a critical comparison of the performance of different water models. *Faraday Discuss.*, 141:251–276, 2009.

[47] John L. Finney. The water molecule and its interactions: the interaction between theory, modelling, and experiment. *Journal of Molecular Liquids*, 90(1):303 – 312, 2001.

[48] Herman Berendsen, J.Raul Grigera, and T P. J. Straatsma. The missing term in effective pair potentials j. 91:6269–6271, 11 1987.

[49] Michael W. Mahoney and William L. Jorgensen. A five-site model for liquid water and the reproduction of the density anomaly by rigid, nonpolarizable potential functions. *The Journal of Chemical Physics*, 112(20):8910–8922, 2000.

[50] Potoff Jeffrey J. and Siepmann J. Ilja. Vapor–liquid equilibria of mixtures containing alkanes, carbon dioxide, and nitrogen. *AIChE Journal*, 47(7):1676–1682.

[51] Nathalia S. V. Barbosa, Yong Zhang, Eduardo R. A. Lima, Frederico W. Tavares, and Edward J. Maginn. Development of an amber-compatible transferable force field for poly(ethylene glycol) ethers (glymes). *Journal of Molecular Modeling*, 23(6):194, May 2017.

Appendix

6.1 Additional plots

6.1.1 C-lattice parameter as a function of loading

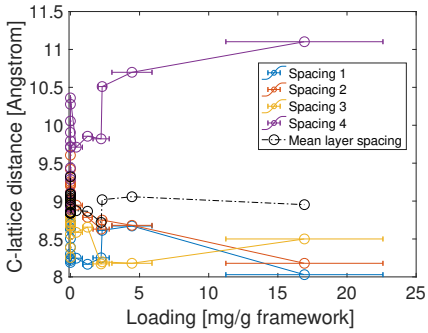

(a) C-lattice parameter as a function of pressure at 273 K

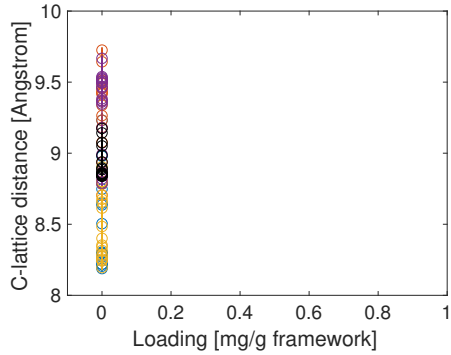

(b) C-lattice parameter for the SPC/E water model as a function of loading at 293 K

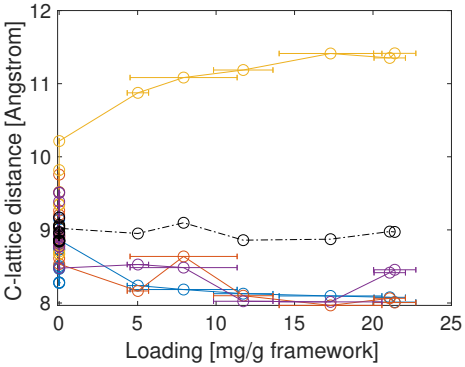

(c) C-lattice parameter as a function of pressure at 313 K

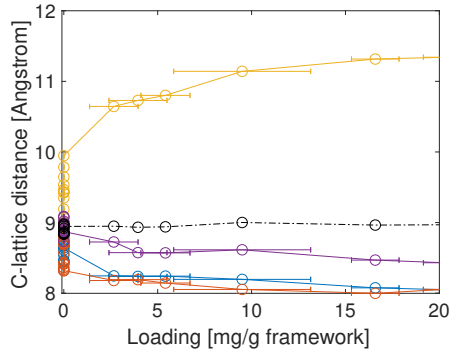

(d) C-lattice parameter for the SPC/E water model as a function of loading at 333 K

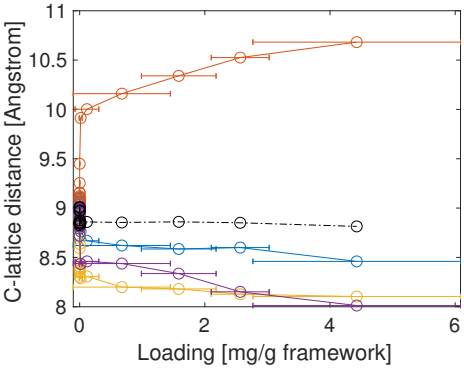

(e) C-lattice parameter as a function of pressure at 353 K

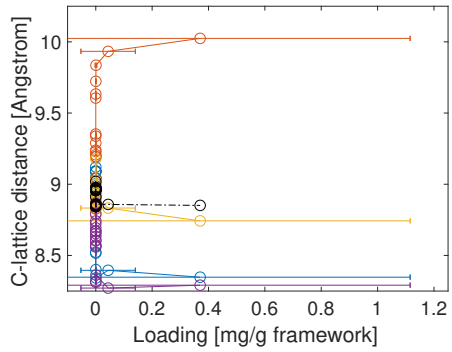

(f) C-lattice parameter for the SPC/E water model as a function of loading at 373 K

Figure 6.1: C-lattice parameter as a function of loading for CO_2, for all temperatures.

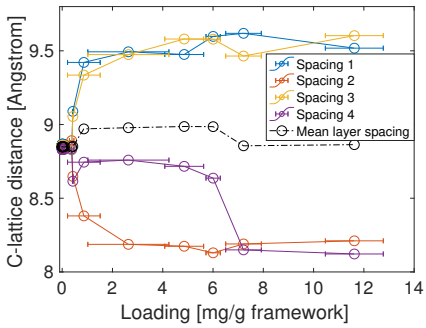

(a) C-lattice parameter as a function of pressure at 273 K

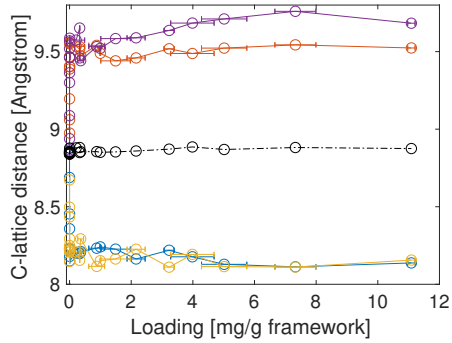

(b) C-lattice parameter for the SPC/E water model as a function of loading at 293 K

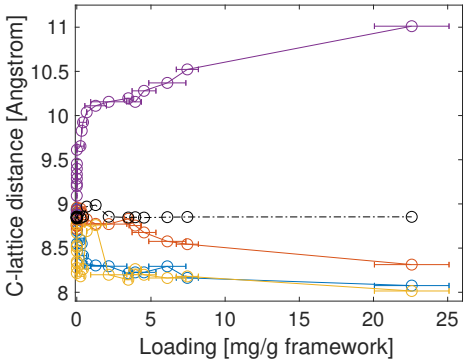

(c) C-lattice parameter as a function of pressure at 313 K

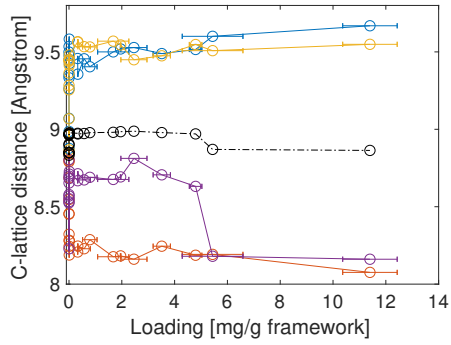

(d) C-lattice parameter for the SPC/E water model as a function of loading at 333 K

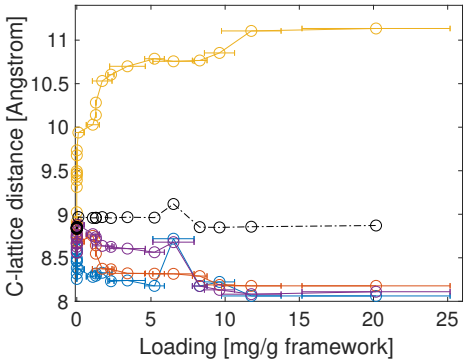

(e) C-lattice parameter as a function of pressure at 353 K

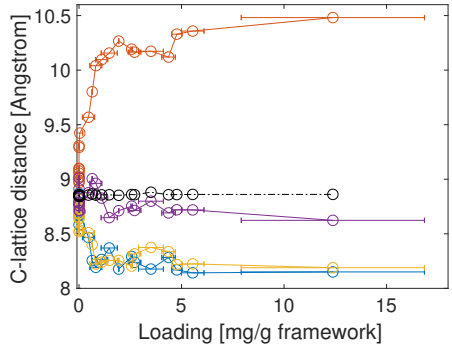

(f) C-lattice parameter for the SPC/E water model as a function of loading at 373 K

Figure 6.2: C-lattice parameter as a function of loading for the SPC/E water model, for all temperatures.

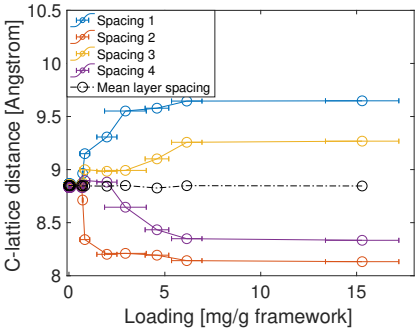

(a) C-lattice parameter as a function of pressure at 273 K

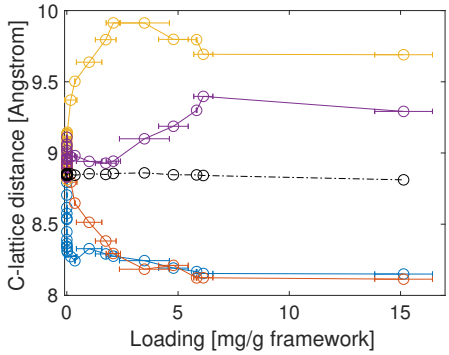

(b) C-lattice parameter for the TIP5p water model as a function of loading at 293 K

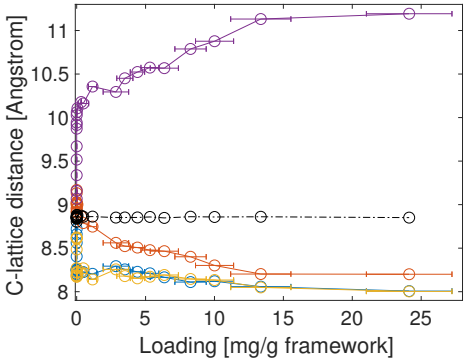

(c) C-lattice parameter as a function of pressure at 313 K

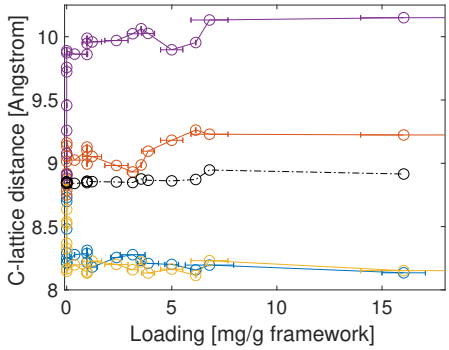

(d) C-lattice parameter for the TIP5p water model as a function of loading at 333 K

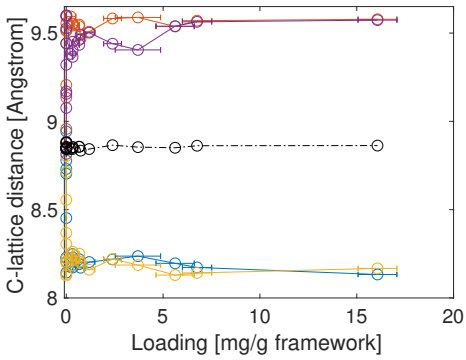

(e) C-lattice parameter as a function of pressure at 353 K

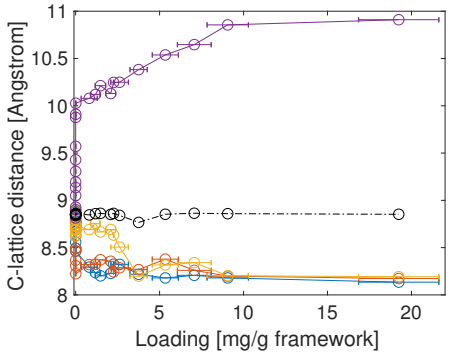

(f) C-lattice parameter for the TIP5p water model as a function of loading at 373 K

Figure 6.3: C-lattice parameter as a function of loading for the TIP5p water model, for all temperatures.

6.1.2 Heat of adsorption calculated by RASPA

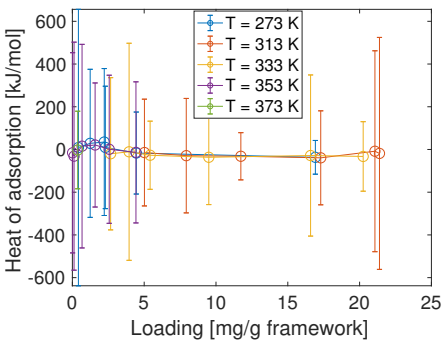

(a) Heat of adsorption for CO_2

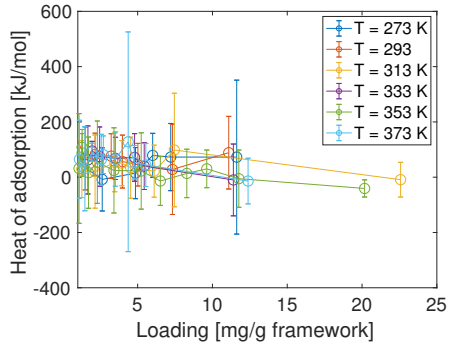

(b) Heat of adsorption for the SPC/E water model

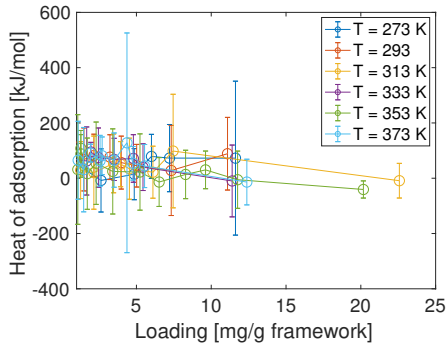

(c) Heat of adsorption for the TIP5p water model.

Figure 6.4: Haat of adsorption for the adsorbed molecules calculated by RASPA